A Radial Space Division Based Evolutionary Algorithm for Many-Objective Optimization

Cheng He[a], Ye Tian[b], Yaochu Jin[c,d], Xingyi Zhang[b], Linqiang Pan[a,e,*]

[a] *School of Automation, Huazhong University of Science and Technology, Wuhan 430074, China*
[b] *School of Computer Science and Technology, Anhui University, Hefei 230039, China*
[c] *Department of Computing, University of Surrey, Guildford, Surrey, GU2 7XH, United Kingdom*
[d] *College of Information Sciences and Technology, Donghua University, Shanghai 201620, China*
[e] *School of Electric and Information Engineering, Zhengzhou University of Light Industry, Zhengzhou 450002, China*

Abstract

In evolutionary many-objective optimization, diversity maintenance plays an important role in pushing the population towards the Pareto optimal front. Existing many-objective evolutionary algorithms mainly focus on convergence enhancement, but pay less attention to diversity enhancement, which may fail to obtain uniformly distributed solutions or fall into local optima. This paper proposes a radial space division based evolutionary algorithm for many-objective optimization, where the solutions in high-dimensional objective space are projected into the grid divided 2-dimensional radial space for diversity maintenance and convergence enhancement. Specifically, the diversity of the population is emphasized by selecting solutions from different grids, where an adaptive penalty based approach is proposed to select a better converged solution from the grid with multiple solutions for convergence enhancement. The proposed algorithm is compared with five state-of-the-art many-objective evolutionary algorithms on a variety of benchmark test problems. Experimental results demonstrate the competitiveness of the proposed algorithm in terms of both convergence enhancement and diversity maintenance.

*Corresponding author.
Email address: lqpan@mail.hust.edu.cn (Linqiang Pan)

Keywords: Many-objective optimization, radial projection, diversity maintain, grid division, multi-line distance minimization problem.

1. Introduction

Real-world optimization problems always involve more than three often conflicting objectives, e.g., cold start engine calibration optimisation [1], risk design optimization [2], and groundwater monitoring network design [3]. These optimization problems are called many-objective optimization problems (MaOPs) [4, 5, 6] and they can be described as follows

$$\begin{aligned} \text{Minimize} \quad & F(x) = (f_1(x), f_2(x), \ldots, f_m(x)) \\ \text{subject to} \quad & \mathbf{x} \in X, \end{aligned} \tag{1}$$

where m is the number of objectives and $X \subseteq \mathbb{R}^D$ is the decision space with $\mathbf{x} = (x_1, x_2, \ldots, x_D)$ being the D-dimensional decision vector [7, 8]. Due to the conflicting nature of the objectives, there does not exist a single solution that can optimize all the objectives simultaneously. Instead, a set of trade-off solutions that cannot be optimized in any objective without degenerating at least one other objective can be achieved, which are also called as Pareto optimal solutions. The collection of all Pareto optimal solutions is the Pareto optimal set (PS), and the image of the PS in objective space is called the Pareto optimal front (PF) [9].

Evolutionary algorithms (EAs) are able to obtain a set of solutions in a single run due to their population-based property, which is suitable for many-objective optimization [10]. In the past two decades, plenty of Pareto-based multi-objective evolutionary algorithms (MOEAs) were developed for solving problems with two to three objectives, e.g., NSGA-II [11], SPEA2 [12], SMEA [13], MOEA/PC [14], and PESAII [15]. However, their efficiency degenerated seriously on problems with more than three objectives (MaOPs as defined) [16], which mainly due to the loss of selection pressure, i.e. the pressure pushes the population towards the PF, when the Pareto-based selection criterion was adopted to select solutions from the population [10, 17].

To enhance the performance of conventional MOEAs on solving MaOPs, plenty of many-objective evolutionary algorithms (MaOEAs) have been proposed in recent years, which can be roughly divided into three categories.

The first category consists of the Pareto-based convergence enhancement approaches. The most intuitive idea for convergence enhancement in Pareto-based MOEAs was to modify the Pareto dominance relationship to increase the selection pressure, and plenty of modified dominance definitions were proposed, e.g., fuzzy dominance [18], ϵ-dominance [19], RP-dominance [20], and preference rank order [21]. Besides, another idea for convergence enhancement was to adopt an additional convergence-related criterion after the use of Pareto dominance based criterion, e.g., the concept of "knee point" in KnEA [22] and the "grid-dominance" relationship in GrEA [23].

The second category consists of the reference-based approaches, where solutions were selected based on the given reference information. For example, in NSGA-III [24], reference vectors were used to select preferred solutions during the environmental selection for many-objective optimization. There were also other algorithms in this category, e.g., MOEA/D [9], MOEA/DD [25], MOEA/D-DU [26], RVEA [17], and PICEA-g [27].

The third category consists of the performance indicator based approaches, where the performance indicators were applied for assessing the quality of each solution to distinguish different candidate solutions in many-objective optimization, e.g., IBEA [28], SMS-MOEA [29], HypE [30], MOMBI-II [31], and MOEA/IGD-NS [32].

There were also several MaOEAs not included in the above three categories. For instance, an MaOEA named Two_Arch2 was proposed for many-objective optimization by maintaining two archives with an indicator-based and a Pareto-based selection principles [33]; LMEA [34] used the decision variable clustering method to divide the decision variables into two different types for solving MaOPs with large-scale decision variables; NMPSO adopted the techniques in swarm intelligence for many-objective optimization [35].

Generally speaking, the above mentioned MaOEAs mainly take the conver-

gence enhancement as the primary criterion, then take the diversity maintenance as the second criterion for many-objective optimization. In other words, most known MaOEAs emphasize the convergence enhancement, but pay less attention to diversity maintenance for many-objective optimization [36]. However, some less converged solutions are important to the diversity of the population, which can help the algorithm to approximate the Pareto front [37]. In this sense, diversity outweighs convergence and should be emphasized for many-objective optimization [38]. In what follows, known diversity maintenance strategies are briefly reviewed and analyzed.

Known diversity maintenance strategies in multi- and many-objective optimization can be roughly divided into four types. The first type of diversity maintenance strategies estimates the crowding degree of a solution based on the distances from this solution to its neighboring solutions, e.g., crowding distance computation in NSGA-II [11], the truncation strategy for archive update in SPEA2 [12], and the weighted distance calculation in KnEA [22]. These strategies are capable of selecting a set of evenly distributed solutions in the objective space but the convergence of the solutions are not considered, which may result in a set of evenly distributed but poorly converged solutions.

The second type consists of the region division based strategies, where the objective space is divided into different hypercubes or subregions with each solution being assigned a crowding degree according to the number of solutions in the same hypercube or subregion, e.g., the region-based approach in PESAII [15], the grid division method in GrEA [23], and the region division based on the geometric information of the Pareto front method in RdEA [37]. There are mainly two drawbacks for these diversity maintenance strategies. First, it is difficult to decide the number of divisions for generating a number of subregions (hypercubes) similar to the population size, since these region division based strategies cannot generate an arbitrary number of hypercubes or subregions in the high-dimensional objective space. For instance, assume the division number in each objective is k in GrEA [23] for an MaOP with m objectives, then k^m hypercubes are formed in the objective space. It turns out that the population

size N is far less than the number of hypercubes ($\geq 2^{10}$) if $N < 1000$, $k \geq 2$ and $m \geq 10$. Second, it is sometimes difficult to maintain a population with constant population size as the number of nonempty subregions (hypercubes) may vary along with the evolution.

The third type of strategies adopts a totally different idea for diversity maintenance, where the reference information (reference vectors, reference points or preference information) is used to select preferred solutions for diversity maintenance, and many algorithms adopt this idea, e.g., NSGA-III [24], MOEA/D [9], I-DBEA [39], MOEA/DD [25], PICEA-g [27], and RVEA [17]. For these reference-based diversity maintenance strategies, they fail to maintain diversity on problems with irregular PFs (degenerated, discontinuous, and convex) [17], since they have predefined the reference information for diversity maintenance without any prior knowledge about the PFs of the problems. For instances, MOEA/D works well on problems with regular PFs (e.g., DTLZ1 to DTLZ4), but fails on problems with irregular PFs (e.g., DTLZ5 to DTLZ7 and WFG1 to WFG9) [17].

The forth type involves the methods adopting data visualization, e.g., the Polar coordinates in MOEA/PC [14], the self organizing mapping in MOEA/D-SOM [40], and SMEA [13]. These methods have improved the performance of MOEAs on diversity maintenance for problems with irregular Pareto fronts [40]. However, the computational cost for the visualization approaches could be expensive and should be applied for multi-objective optimization problems only. For instance, MOEA/PC and SMEA are designed for multi-objective optimization, and their runtime on many-objective problems is unbearable.

In this work, a radial projection based diversity maintenance strategy is proposed for many-objective optimization. In the proposed strategy, the solutions in the high-dimensional objective space are first projected to the 2-dimensional radial space. Second, an adaptive grid division approach is applied to divide the region occupied by these projected solutions into a number of identical rectangles. Note that this adaptive grid division procedure does not suffer from the difficulty that conventional region division based diversity maintenance strate-

gies have, as this adaptive grid division is operated in the 2-dimensional radial space, and the division in each dimension can be easily set as $\lfloor\sqrt{N}\rfloor$, where N is the population size. Thirdly, an adaptive penalty based approach is used to select a better converged solution from the grid with multiple solutions for convergence enhancement, where the penalty fitness function is constructed based on the combination of the crowding degree of the solution (in the radial space) and its convergence degree (in the objective space). Compared with the conventional diversity maintenance strategy, the convergence of the population is considered in the proposed strategy to avoid the convergence degeneration, and the proposed diversity strategy is of high efficiency due to the reduction in dimensionality. Meanwhile, since no reference information is introduced to select preferred solutions, the problem of unsuitably predefined reference information does not exist in the proposed strategy.

Based on the radial projection based diversity maintenance strategy, a radial space division based many-objective evolutionary algorithm, called RSEA, is proposed. The main contributions of this work are summarized as follows.

1. An MaOEA with the radial projection based diversity maintenance strategy is proposed for many-objective optimization. In the proposed algorithm, the high-dimensional solutions are projected to the 2-dimensional radial space for environmental selection and mating selection, where the diversity of the population is emphasized. It is worth noting that the distribution condition of the projected solutions is similar to that in the high-dimensional objective space as we have verified, hence the diversity of the population can be maintained efficiently by the radial projection based diversity maintenance strategy.
2. An adaptive grid division strategy is applied to the radial projected solutions during the environmental selection for selecting a set of uniformly distributed and well converged solutions to form the population for the next generation, the crowding degrees of solutions together with their convergence degrees are considered for selecting a set of well converged and

uniformly distributed solutions. This selection strategy can eliminate the negative impact of the curvature information lost on the performance of RSEA, where the loss of curvature information is caused by the dimensionality reduction during the radial projection.

3. In the proposed RSEA, all the parameters involved are adaptively adjusted, which enhances the practicability of RSEA for solving real-world application problems.

4. Extensive experimental results are conducted to verify the performance of RSEA by comparing it with five state-of-the-art MaOEAs on a variety of benchmark problems. Empirical results demonstrate that RSEA is efficient in diversity maintenance, and it holds a competitive performance on many-objective optimization compared with known MaOEAs.

The rest of this paper is organized as follows. In Section 2, the radial projection with its advantages and shortcomings is discussed. The proposed RSEA for many-objective optimization is described in Section 3. Experimental settings and the performance of RSEA compared with five state-of-the-art methods on the benchmark problems are presented in Section 4. Conclusions and future work are given in Section 5.

2. Related Works and Radial Projection

In this section, we first introduce some related works on data visualization, followed by the details of the radial projection. Then the ability of radial projection on reflecting the distribution of high-dimensional solutions in the radial space is analyzed. Next, the advantages and shortcomings of the radial projection are discussed.

2.1. Related Works and Radial Projection

Visualization of population in a high-dimensional objective space provides researchers an intuitive view of the quality of the solutions in terms of convergence and diversity, which also presents an opportunity that could be well

exploited in designing MaOEAs [41, 42]. Plenty of visualization methods have been proposed, e.g., the Buddle chart [43], self organizing maps (SOM) [44], parallel coordinates [45], Isomap [46], Sammon mapping [47], Radial coordinate visualization [48], Polar coordinates [14], and t-SNE [49]. They can be roughly classified as two types, i.e., visualization based on parallel coordinate system (e.g., parallel coordinates and heatmap [50]) and visualization based on mapping (e.g., SOM, t-SNE, Sammon mapping, and Isomap).

These visualization methods have been proved to be efficient on reflecting the distribution condition and crowding degree of the high-dimensional points, but not all the visualization methods are suitable for designing MaOEAs. For the visualization methods based on parallel coordinate system, the neighbourhood information of the points is not clear (e.g., parallel coordinates and heatmap), and they can hardly be applied for diversity enhancement. As for the mapping based methods, some could be computationally expensive (e.g., t-SNE and Sammon mapping); while others may over emphasize the clustering of similar points and the separation of dissimilar points, which are too strong for reflecting the crowding degree of solutions in many-objective optimization (e.g., t-SNE and Isomap).

The radial coordinate visualization (RadViz) [48] belongs to the second type of visualization methods. The radial projection method in RadViz is computationally cheap, and the distribution and crowding conditions of the entire set of points are reserved (this will be proved in the following). Hence, the radial projection is adopted in this work for designing an algorithm for many-objective optimization.

Radial projection was first applied to visualize the distribution of DNA sequences for data mining in the field of bioinformatics [48], then it was used to visualize the final distribution of obtained solutions in the area of many-objective optimization [51, 42, 52, 53]. The basic idea of the radial projection is to project the high-dimensional points into a 2-dimensional radial space by two projection weight vectors. Assume $A = (a_1, a_2, \ldots, a_m)$ is an m-dimensional point with $a_i \in [0, 1]$ (here we restrict the range of each dimension to $[0, 1]$,

since the normalization operation can be adopted before the radial projection), and the two weight vectors W_1, W_2 are defined as follows:

$$W_1 = (\cos(\theta_1), \cos(\theta_2), \ldots, \cos(\theta_m))^T,$$
$$W_2 = (\sin(\theta_1), \sin(\theta_2), \ldots, \sin(\theta_m))^T,$$

where θ_i is the angle corresponding to dimension i and $\theta_i = 2\pi(i-1)/m$. Then the coordinate of point A in the radial space is denoted as $Y = (y_1, y_2)$, where $y_1 = AW_1(A\mathbf{1})^{-1}$, $y_2 = AW_2(A\mathbf{1})^{-1}$, and $\mathbf{1}$ is an $m \times 1$ all-one vector.

In what follows, we illustrate how radial projection reflects the distribution of high-dimensional points in the 2-dimensional radial space. Suppose two points $X_1, X_2 \in \Omega^m$, where Ω is a m-dimensional space, and their coordinates in the radial space are Y_1 and Y_2, respectively. In space Ω^m, the Euclidean distance from X_1 to X_2 is $E_m = ||X_1 - X_2||$, and the Euclidean distance from Y_1 to Y_2 in the radial space is $E_2 = ||Y_1 - Y_2||$. Then we have

$$\begin{aligned} E_2 &= ||Y_1 - Y_2|| \\ &= ||(X_1W_1(X_1\mathbf{1})^{-1}, X_1W_2(X_1\mathbf{1})^{-1}) - (X_2W_1(X_2\mathbf{1})^{-1}, X_2W_2(X_2\mathbf{1})^{-1})|| \\ &= ||(((X_1I)^{-1}X_1 - (X_2I)^{-1}X_2)W_1, ((X_1I)^{-1}X_1 - (X_2I)^{-1}X_2)W_2)||. \end{aligned}$$

Let $L = (X_1\mathbf{1})^{-1}X_1 - (X_2\mathbf{1})^{-1}X_2 = (l_1, l_2, \ldots, l_m)$, then

$$\begin{aligned} E_2 &= ||(LW_1, LW_2)|| \\ &= \sqrt{(LW_1, LW_2)((LW_1)^T, (LW_2)^T)^T} \\ &= \sqrt{LW_1W_1^TL^T + LW_2W_2^TL^T} \\ &= \sqrt{L(W_1W_1^T + W_2W_2^T)L^T}. \end{aligned}$$

Assume $R = W_1W_1^T + W_2W_2^T$, then we have

$$R = \begin{bmatrix} a_{11} & a_{12} & \cdots & a_{im-1} & a_{1m} \\ & & \cdots & & \\ a_{i1} & \cdots & a_{ij} & \ldots & a_{im} \\ & & \cdots & & \\ a_{m1} & a_{m2} & \ldots & a_{mm-1} & a_{mm} \end{bmatrix}, \quad (2)$$

where

$$\begin{aligned} a_{ij} &= \cos(\theta_i)\cos(\theta_j) + \sin(\theta_i)\sin(\theta_i) \\ &= \cos(\theta_i - \theta_j). \end{aligned}$$

Hence,

$$\begin{aligned} E_2 &= \sqrt{LRL^T} \\ &= \sqrt{\sum_{j=1}^{m} l_j \left(\sum_{i=1}^{m} l_i \cos(\theta_i - \theta_j) \right)} \\ &= \sqrt{\underbrace{\sum_{j=1}^{m} l_j^2}_{\text{Part I}} + \underbrace{\sum_{i \neq j}^{i,j \in [1,m]} l_i l_j \cos(\theta_i - \theta_j)}_{\text{Part II}}}. \end{aligned} \tag{3}$$

Note that, the "Part I" of E_2

$$\begin{aligned} \sum_{j=1}^{m} l_j^2 &= LL^T \\ &= (X_1\mathbf{1})^{-2} X_1 X_1^T - (X_1\mathbf{1})^{-1}(X_2\mathbf{1})^{-1} X_1 X_2^T \\ &- (X_1\mathbf{1})^{-1}(X_2\mathbf{1})^{-1} X_2 X_1^T + (X_2\mathbf{1})^{-2} X_2 X_2^T \end{aligned}$$

is linearly approximate to

$$E_m = X_1 X_1^T - X_1 X_2^T - X_2 X_1^T + X_2 X_2^T.$$

While "Part II" of E_2 is the weighted sum of different objectives in $X_1 - X_2$, and it effects less to E_2 than "Part I" as $cos(\theta_i - \theta_j) < 1$ with $i \neq j$.

It can be concluded that the Euclidean distance of arbitrary pairwise points in high-dimensional space is similar to that of the projected pairwise points in the radial space. Hence, the radial projection is capable of reflecting the distribution of high-dimensional points in the 2-dimensional radial space.

2.2. Ability Analysis

To take a closer look at the differences between the high-dimensional visualization (parallel coordinates) and the RadViz by radial projection, several

examples with different structures of Pareto fronts are used to analyze the ability of radial projection on reflecting the distribution of high-dimensional points in the 2-dimensional radial space. The distribution of points on the convex, flat, and concave complete Pareto fronts are displayed in Fig. 1 (a), (b), and (c), respectively, where a complete Pareto front means the Pareto front is a continuous hypersurface. In this figure, the RadViz of three different Pareto fronts are the same, where the curvature information of the Pareto fronts is missing by radial projection but the spread situation and density information is reserved. In conclusion, the RadViz is capable of reflecting the crowding degree of each point on complete PFs, and the distribution of high-dimensional points can be reflected by the RadViz.

In Fig. 2, the distribution of high-dimensional points on a discontinuous Pareto front is displayed in parallel coordinates and RadViz, respectively. It can be observed that these points are distributed discontinuously in parallel coordinates, but they are continuously distributed in RadViz, which means the diversity maintenance in radial space can be much easier than that in high-dimensional objective space even with the loss of information in discontinuous region.

To explore the ability of RadViz on reflecting the distribution of points on degenerated Pareto fronts, three examples of 275 10-dimensional uniformly distributed points on convex, flat, and concave degenerated Pareto fronts are displayed in parallel coordinates and RadViz in Fig. 3, respectively. It can be observed that the curvature information of the Pareto fronts is missing in RadViz, while the density information and distribution of the points are reserved. It turns out that this RadViz is capable of reflecting the distribution condition of high-dimensional solutions in radial space, where the points are distributed on the degenerated Pareto fronts.

To summarize, the RadViz is capable of reflecting the distribution of high-dimensional points in the 2-dimensional radial space. Hence the radial projection can be applied to maintain diversity in many-objective optimization. Nevertheless, the curvature information of the Pareto front as well as the con-

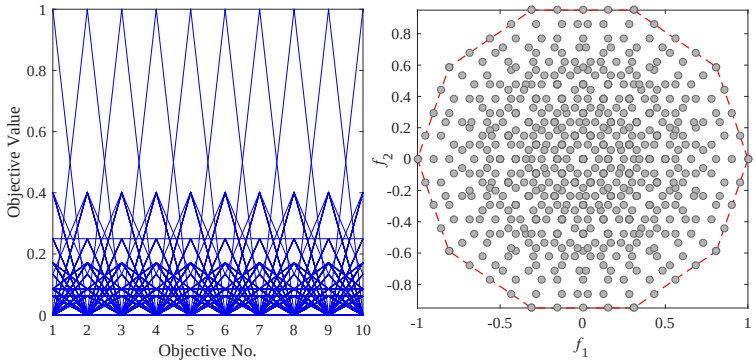

(a) The distribution of 275 evenly distributed points on a complete convex Pareto front.

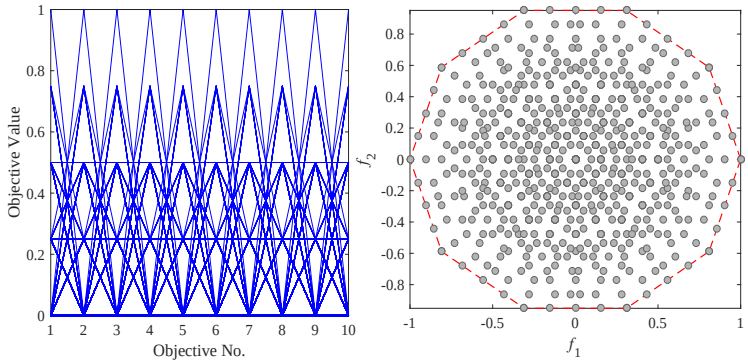

(b) The distribution of 275 evenly distributed points on a complete flat Pareto front.

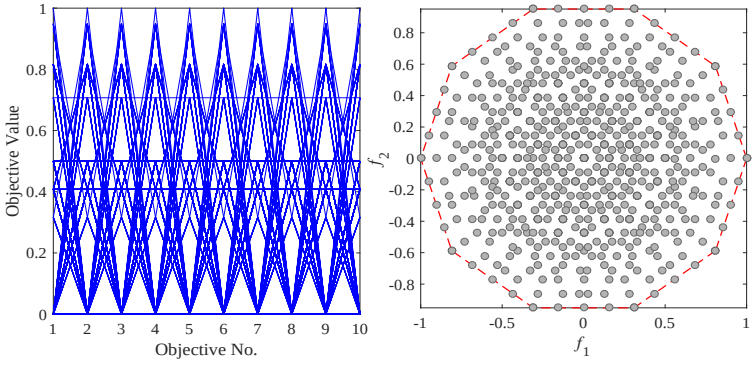

(c) The distribution of 275 evenly distributed points on a complete concave Pareto front.

Figure 1: The distributions of 275 10-dimensional evenly distributed points on different complete Pareto fronts displayed by parallel coordinates and RadViz, respectively.

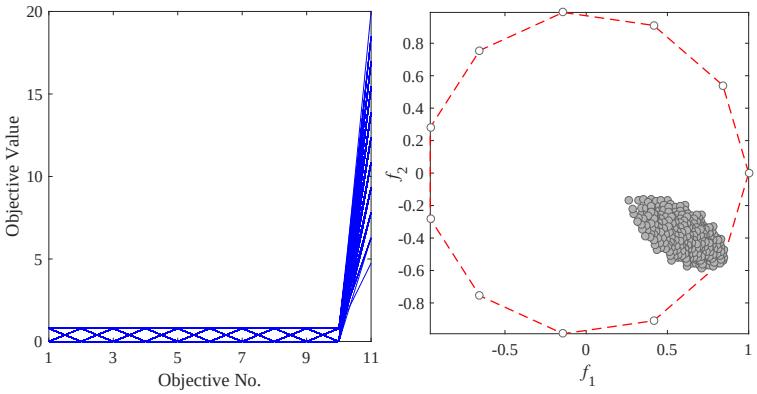

Figure 2: The distribution of 275 10-dimensional evenly distributed points on a discontinuous Pareto front displayed by parallel coordinates and RadViz, respectively.

vergence information of each point is missing after the radial projection, which should be considered for designing high-performance MaOEAs.

3. The Proposed Algorithm RSEA

In this section, we propose a radial space division based many-objective evolutionary algorithm, called RSEA. Firstly, the general framework of RSEA is presented. Then, the details of the components of RSEA, the adaptive grid division in radial space, the mating pool selection, and the environmental selection, are given.

3.1. General Framework of RSEA

The framework of the proposed RSEA is similar with that of NSGA-II, which is shown in Algorithm 1 in pseudo code. First, N individuals are randomly generated to form the initial population P_0. Second, solutions in P_0 are projected to the 2-dimensional radial space, and a binary tournament strategy is applied to select individuals from P_0 for generating offspring individuals using a variation method. In the mating selection procedure, two tournament metrics are adopted, namely, the rectangle crowding degree (in radial space) and convergence degree (in objective space). Thirdly, non-dominated sorting is

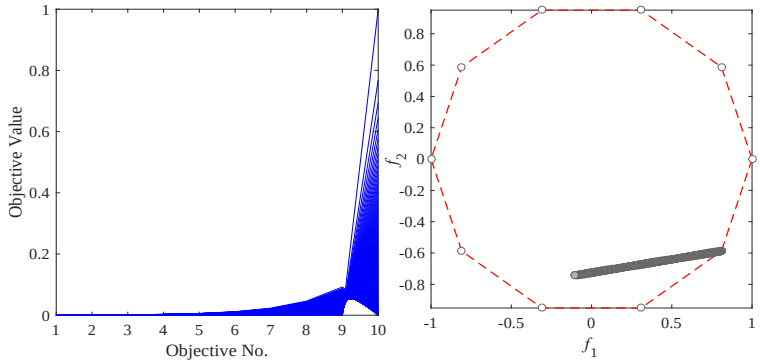

(a) The distribution of 275 solutions on a degenerated convex Pareto front.

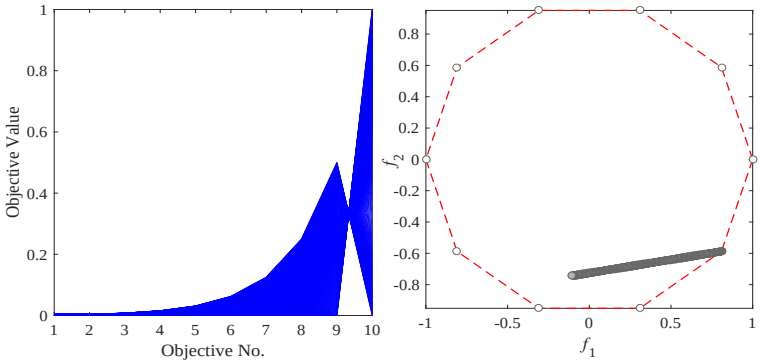

(b) The distribution of 275 solutions on a degenerated flat Pareto front.

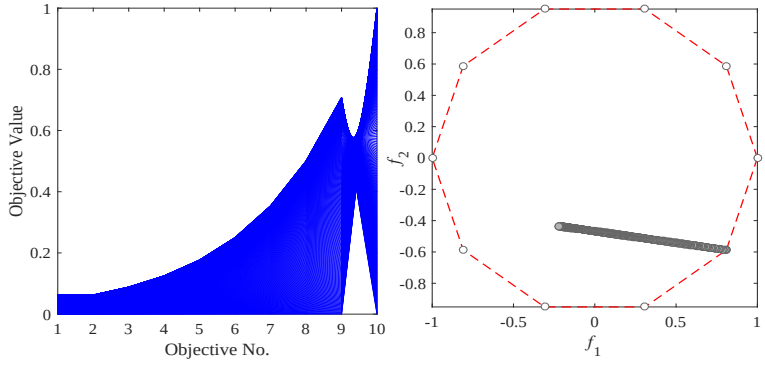

(c) The distribution of 275 solutions on a degenerated concave Pareto.

Figure 3: The distributions of 275 10-dimensional evenly distributed points on the degenerated convex, flat, and concave Pareto fronts displayed by parallel coordinates and RadViz, respectively.

performed on the combination of parent and offspring population, followed by the adaptive grid division based selection in radial space to select N individuals as the parent population for the next generation. This procedure repeats until the termination condition is satisfied.

Algorithm 1 General Framework of RSEA

Input:

N (size of population).

1: $P_0 \leftarrow Initialization(N)$
2: **while** termination criterion not fulfilled **do**
3: $G \leftarrow Radial\_Grid(P_0, N))$
4: $P \leftarrow Mating\_Selection(P_0, G)$
5: $P' \leftarrow Variation(P, N)$
6: $P_0 \leftarrow Envionmental\_Selection(P' \cup P, N)$
7: **end**
8: **Return:** P_0

The main differences between NSGA-II and RSEA are the mating pool selection and environmental selection. In NSGA-II, solutions with better Pareto dominance rankings and larger crowding distances are selected in mating selection and environmental selection [11]; however, in RSEA the solutions in high-dimensional objective space are first projected to the 2-dimensional radial space, and these projected solutions are located in different rectangles by an adaptive grid division approach, then the better converged solutions in the less crowed rectangles are selected as parent individuals in mating selection, while an adaptive penalty based approach is applied to select diversity-related and well converged solutions during the environmental selection in RSEA.

In what follows, we will show the details of the components of RSEA including adaptive grid division in radial space, binary mating selection, and environmental selection.

3.2. Adaptive Grid Division in Radial Space

A grid is used as frame to determine the locations of individuals in the radial space, which is important in RSEA for estimating the crowding condition of each solution in current population. To enhance the accuracy of the grid for estimating the crowding condition of each solution, its adaptability with the evolutionary population seems to be advisable. In other words, the location of the grid should be adaptively adjusted along with the evolution of the population.

The details of the adaptive grid division in radial space are shown in Algorithm 2. First, the objective vectors of current population are normalized according to their ideal and nadir points of all the non-dominated solutions in the population. Second, the normalized objective vectors are projected from the high-dimensional objective space to the 2-dimensional radial space by the projection weight vectors. Thirdly, the lower and upper boundaries of the projected solutions are calculated to form the rectangle of the area occupied by these solutions. Then the rectangle is divided into $(\lfloor\sqrt{N}\rfloor)^2$ identical grids with each rectangle side divided into $\lfloor\sqrt{N}\rfloor$ divisions, where N is the population size. Finally, the coordinate of each solution in radial space and its grid label in the divided rectangle are calculated.

3.3. Mating Selection

The mating selection in RSEA employs a binary tournament selection strategy using two tournament metrics, namely, the grid crowding degree (in the radial space) and the convergence degree (in the objective space). The mating selection begins with the rectangle crowding degree tournament selection, where N nonempty rectangles are selected based on the crowding degree of each rectangle. Here, the crowding degree of a rectangle is defined as the number of points in the same rectangle as shown in Eq. (4).

$$Crowd(G_S) = |S|, \tag{4}$$

where S is the set of solutions located in rectangle G_S and $|*|$ denotes the number of elements in set $*$. Then the better converged solution in each rectangle is

Algorithm 2 *Radial_Grid*

Input:

F (objective vectors), N (population size).

Output:

Y (coordinate in radial space), G (rectangle labels).

$P_N \leftarrow$ Normalize the objective vectors of P
for $i = 1 : m$ **do**
  $\theta_i \leftarrow 2\pi(i-1)/m$ /*m is the number of objectives*/
end
$W_1 \leftarrow (\cos(\theta_1), \ldots, \cos(\theta_m))$,
$W_2 \leftarrow (\sin(\theta_1), \ldots, \sin(\theta_m))$
$Y \leftarrow (FW_1, FW_2)$
$d \leftarrow \lceil \sqrt{N} \rceil$ /*Division number in each dimension*/
$B_l \leftarrow \min Y$,$B_u \leftarrow \max Y$
$G \leftarrow \lfloor d(Y - B_l)/(B_u - B_l) \rfloor$

selected to the mating pool by binary tournament selection, where the convergence degree of a solution is defined as the Euclidean length of the normalized objective vector as given in Eq. (5).

$$Con(F_i) = \left|\left| \frac{F_i - F_{min}}{F_{max} - F_{min}} \right|\right|, \tag{5}$$

where F_i is the objective vector of the ith individual and F_{min}, F_{max} are the ideal and nadir point respectively. Algorithm 3 illustrates the detailed procedure of the mating selection in RSEA in pseudo code.

It is worth noting that, this mating pool selection strategy emphasises the selection of diversity-related solutions for enhancing the diversity maintenance, followed by the selection of convergence-related solutions to enhance the convergence of the population.

3.4. Environmental Selection

Environmental selection is used to select fitter solutions as parents for the next generation in RSEA. It shares a similar mechanism to the environmental

Algorithm 3 *Mating_Selection*

Input:

P (population), G (rectangle labels).

Output:

H (mating pool population)

$Q, H \leftarrow \emptyset$
$Crowd \leftarrow$ Calculate the crowding degrees of solutions in P by to Eq. (4)
$Con \leftarrow$ Calculate the convergence degrees of solutions in P by to Eq. (5)
while $|Q| < |P|$ **do**
  Randomly select two rectangles a and b from G
  if $Crowd(a) < Crowd(b)$ **then**
    $Q \leftarrow Q \cup \{a\}$
  else
    $Q \leftarrow Q \cup \{b\}$
  end
end
for $i \leftarrow 1 : |P|$ **do**
  $S \leftarrow$ Find the solutions in the ith rectangle in Q
  Randomly select two solutions w and v from S
  if $Con(w) < Con(v)$ **then**
    $H \leftarrow H \cup \{w\}$
  else
    $H \leftarrow H \cup \{v\}$
  end
end

selection in NSGA-II, where N individuals are selected from the combination of offspring population and parent population in current generation. Although NSGA-II and RSEA both adopt the Pareto dominance as the primary criterion in environmental selection, RSEA adopts a radial projection based grid division selection strategy as the second criterion instead of the crowding distance based criterion as NSGA-II does. Besides, the qualities of the solutions in the same rectangle is assessed by the minimum Euclidean distance to the selected solutions in radial space together with its convergence degree. The environmental selection in RSEA is shown in Algorithm 4.

Algorithm 4 *Environmental_Selection*

Input:

P (population), N (population size).

Output:

Q (population).

$Q \leftarrow \emptyset$

$(F_1, F_2, \dots) \leftarrow$ Non-dominated-sort(P)

$P \leftarrow F_1 \cup F_2 \cup \cdots \cup F_i$

/*$|F_1 \cup \cdots \cup F_{i-1}| < N$, $|F_1 \cup \cdots \cup F_i| \geq N$*/

$[Y, G] \leftarrow Radial\_Grid(P, N)$

$C \leftarrow 0$ /*Initialize the crowding degree*/

$Q \leftarrow$ Select the extreme solutions in P

$C_Q \leftarrow 1$ /*Update the crowding degrees*/

while $|Q| < N$ **do**

  $K \leftarrow \arg\min C$ /*Find solutions in the least crowded rectangles*/

  $Fit(K, Q) \leftarrow$ Calculate the fitness values of solutions in K by Eq. (6)

  $P_q \leftarrow \arg_{q \in K} \min Fit(K, Q)$

  $Q \leftarrow Q \cup \{P_q\}$

  $P \leftarrow P \backslash \{P_q\}$ /*Delete the selected solution*/

  $C_q \leftarrow C_q + 1$ /*Update the crowding degree*/

end

The details of the environmental selection in RSEA are illustrated as follows. First, current population is sorted by the efficient non-dominated sorting approach proposed in [54], and solutions before and belonged to the last Pareto front (the size is equal to N or for the first time exceeds N) are selected to form population P. Second, the solutions in P are projected to the 2-dimensional radial space and their coordinates in the radial space as well as their locations in the divided grid are worked out by Algorithm 2. Thirdly, m extreme solutions of population P are selected to population Q and the corresponding crowding degrees are updated, where m is the number of objectives. Fourthly, $N - m$ remaining solutions in P are selected one by one according to the crowding degrees of their locating rectangles and their fitness values as illustrated in Algorithm 4 from step 9 to step 16. The fitness function for estimating the qualities of different solutions is defined as Eq. (6).

$$Fit(X, Q) = Con(X) \cdot r \cdot m - \min ||Y(X) - Y(Q)||, \tag{6}$$

where Q is the set of selected solutions and $Con(X)$ is the convergence degree of solution X according to Eq. (5) with $Y(*)$ denoting the coordinate of solution $*$ in the radial space. In this equation, the penalty parameter r is adaptively adjusted along with the evaluation of the population, where $r = 1 - (t/t_{max})^2$ with t being the number of evaluated solutions and t_{max} is the maximum number of evaluations. In this adaptive penalty based approach, the construction of the fitness function takes both the density condition of the solution (in the radial space) and its convergence degree (in the objective space) into considering to take full advantage of the ability of the radial projection, and to avoid the shortcoming of the convergence information lost caused by radial projection. Meanwhile, the adaptive penalty parameter r enhances the convergence maintenance at the early stage of the evolution and enhances the diversity maintenance when the solutions are well converged.

An example is given in Fig. 4 to illustrate the process of the environmental selection in RSEA. In this figure, 12 solutions in the 6-dimensional objective space are projected to the 2-dimensional radial space, and the radial space is

divided into nine rectangles for selecting nine solutions from these 12 solutions to form the next generation population. Since each extreme solution of the population owns at least one minimum objective value in some objective, they are more likely to be projected to the vertices of the radial space. The environmental selection in RSEA begins with selecting the six extreme solutions and updating the crowding degrees of the corresponding rectangles. Then three solutions are required to be selected from set $\{s_1, s_2, s_3, s_4, s_5, s_6\}$ one by one. First, the most sparsely distributed solution s_4 in radial space is selected due to the fact that its fitness value is the minimum among those of solutions in $\{s_1, s_2, s_3, s_4, s_5, s_6\}$. Then the crowding degree of the rectangle contains solution s_4 is updated. Second, solutions in the rectangles with the minimal crowding degrees are considered, and solutions s_1, s_3, and s_6 are compared as the crowding degrees of their locating rectangles are zero. Afterwards, solution s_1 is selected as its fitness value is smaller than that of the rest solutions, and the crowding degree of the rectangle containing solution s_1 is updated. Finally, solution s_6 is selected as the crowding degree of the rectangle with solution s_6 is minimum among those of solutions in $\{s_3, s_5, s_6\}$. As a result, six extreme solutions and solutions s_1, s_4, and s_6 are selected to form the population for the next generation, which are uniformly distributed in the radial space.

4. Experimental Study and Results

In this section, the performance of RSEA on many-objective optimization is verified by empirically comparing it with five popular MaOEAs, namely, MOEA/D [9], NSGA-III [24], MaOEA-R&D [55], RPD-NSGA-II [20], and PICEA-g [27] on a set of benchmark problems with 3, 5, 10, and 15 objectives.

In what follows, we will first present a brief introduction to the benchmark problems, then the adopted performance indicators are introduced, followed by the parameter settings used in the comparison. Each algorithm is run for 20 runs on each test problem independently, and the Wilcoxon rank sum test is adopted to compare the results achieved by RSEA and other compared algorithms at a

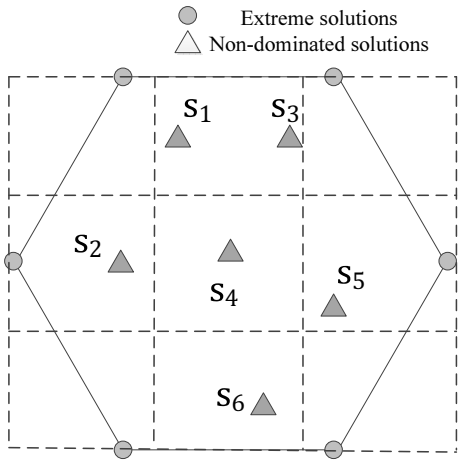

Figure 4: An example to illustrate the process of the environmental selection in RSEA, where nine solutions should be selected from the population with 12 solutions.

significant level of 0.05. Symbol '+' indicates that the compared algorithm is significantly outperformed by RSEA according to the Wilcoxon rank sum test, while '−' represents that RSEA is significantly outperformed by the compared algorithm, and '≈' means that there is no statistically significant difference between the results achieved by RSEA and the compared algorithm.

Then, the impact of the permutation of the radial projection weight vectors is investigated, and the sensitivity of parameter r in RSEA is tested.

Finally, the runtime of the proposed RSEA compared with other five popular algorithms is presented to verify the efficiency of the proposed RSEA. The source codes of all the compared algorithms are written on a Matlab platform named PlatEMO [56] (Matlab version: R2014b 64-bit) to create a fair environment for comparison.

4.1. Test Problems

The first seven test problems are DTLZ1 to DTLZ7 taken from DTLZ test suite [57], where the number of decision variables is shown in Table 1 as recommended in [17] and [22].

Next, test problems WFG1 to WFG9 are adopted from the WFG test suite

Table 1: Settings of Problems DTLZ1 to DTLZ7.

Problem	Number of objectives (M)	Number of variables (D)	Parameter (k)
DTLZ1	3, 5, 10,15	M-1+k	5
DTLZ2,3,4,5,6	3, 5, 10,15	M-1+k	10
DTLZ7	3, 5, 10,15	M-1+k	20

[58], which are designed by introducing non-separability, deception, and bias in decision space as well as mixed geometric structures of the PFs in objective space. The number of decision variables for these WFG problems is shown in Table 2 as recommended in [17] and [22].

Table 2: Settings of Problems WFG1 to WFG9.

Number of Objectives	Position Parameter (K)	Distance Parameter (L)	Number of Variables
3	2	10	$K+L$
5	4	10	$K+L$
10	9	10	$K+L$
15	14	10	$K+L$

Then test problems MaF2, MaF4, and MaF5 are selected from benchmark functions for CEC'2017 competition on evolutionary many-objective optimization, whose PFs are concave, multimodal, and biased, respectively [59].

Finally, the multi-line distance minimization problems (ML-DMPs) are used to test the diversity maintenance of the compared algorithms, where the images of the solutions in objective space are similar to that of the solutions in decision space, where the number of decision variables is two [60].

The formulations of these problems are given as follows, and the number of

decision variables in MaF problems is $n = M + K - 1$ with $K = |\mathbf{x}_M|$ being the number of objectives.

MaF2

$$\begin{cases} f_1(\mathbf{x}) = (1 + g_1(\mathbf{x}_M)) \prod_{i=1}^{M-1} \cos(\theta_i) \\ f_r(\mathbf{x}) = (1 + g_i(\mathbf{x}_M)) \sin(\theta_{M-r+1}) \prod_{j=1}^{M-r} \cos(\theta_j) \\ f_M(\mathbf{x}) = (1 + g_M(\mathbf{x}_M)) \sin(\theta_1) \\ \quad r = 2, \ldots, M-1 \end{cases} \tag{7}$$

with

$$\begin{aligned} g_i(\mathbf{x}_M) &= \sum\nolimits_{j=M+(i-1)\cdot\lfloor\frac{n-M+1}{M}\rfloor}^{M+i\cdot\lfloor\frac{n-M+1}{M}\rfloor-1} ((\frac{x_j}{2} + \frac{1}{4}) - 0.5)^2, \\ g_M(\mathbf{x}_M) &= \sum\nolimits_{j=M+(i-1)\cdot\lfloor\frac{n-M+1}{M}\rfloor}^{n} ((\frac{x_j}{2} + \frac{1}{4}) - 0.5)^2, \\ \theta_i &= \frac{\pi}{2} \cdot (\frac{x_i}{2} + \frac{1}{4}) \text{ for } i = 1, \ldots, M-1. \end{aligned} \tag{8}$$

MaF3

$$\begin{cases} f_1(\mathbf{x}) = [(1 + g(\mathbf{x}_M)) \prod_{i=1}^{M-1} \cos(\frac{\pi}{2} x_i)]^4 \\ f_r(\mathbf{x}) = [(1 + g(\mathbf{x}_M)) \sin(\frac{\pi}{2} x_{M-r+1}) \prod_{j=1}^{M-r} \cos(\frac{\pi}{2} x_j)]^4 \\ f_M(\mathbf{x}) = [(1 + g(\mathbf{x}_M)) \sin(\frac{\pi}{2} x_1)]^2 \\ \quad r = 2, \ldots, M-1 \end{cases} \tag{9}$$

with

$$g(\mathbf{x}_M) = 100[|\mathbf{x}_M| + \sum_{i=1}^{|\mathbf{x}_M|} (x_i - 0.5)^2 - \cos(20\pi(x_i - 0.5))]. \tag{10}$$

MaF4

$$\begin{cases} f_1(\mathbf{x}) = a(1+g(\mathbf{x}_M))(1-\prod_{i=1}^{M-1}\cos(\frac{\pi}{2}x_i))) \\ f_r(\mathbf{x}) = a^r(1+g(\mathbf{x}_M))(1-\sin(\frac{\pi}{2}x_{M-r+1})\prod_{j=1}^{M-r}\cos(\frac{\pi}{2}x_i))) \\ f_M(\mathbf{x}) = a^M(1-\sin(\frac{\pi}{2}x_1))\times(1+g(\mathbf{x}_M)) \\ \quad r=2,\ldots,M-1 \end{cases} \tag{11}$$

with

$$g(\mathbf{x}_M) = 100[|\mathbf{x}_M| + \sum_{i=1}^{|\mathbf{x}_M|}(x_i-0.5)^2 - \cos(20\pi(x_i-0.5))] \text{ and } a=2. \tag{12}$$

MaF5

$$\begin{cases} f_1(\mathbf{x}) = a^M[(1+g(\mathbf{x}_M))\prod_{i=1}^{M-1}\cos(\frac{\pi}{2}{x_i}^{\alpha})]^4 \\ f_r(\mathbf{x}) = a^{M-r+1}[(1+g(\mathbf{x}_M))\sin(\frac{\pi}{2}x_{M-r+1}^{\alpha})\prod_{j=1}^{M-r}\cos(\frac{\pi}{2}{x_j}^{\alpha})]^4 \\ f_M(\mathbf{x}) = a[\sin(\frac{\pi}{2}{x_1}^{\alpha})(1+g(\mathbf{x}_M))]^4 \\ \quad r=2,\ldots,M-1 \end{cases} \tag{13}$$

with

$$g(\mathbf{x}_M) = \sum_{i=1}^{|\mathbf{x}_M|}(x_i-0.5)^2,\ \alpha{=}100, \text{ and } a=2. \tag{14}$$

ML-DMP This function considers a two-dimensional decision space. As its name suggests, the objectives of a solution $\mathbf{x}=(x_1,x_2)$ are the Euclidean distance from $\mathbf{x}$ to a set of M target points $(A_1, A_2, \ldots, A_M)$ of a given polygon, which should be minimized simultaneously. It can be formulated as

$$\begin{cases} f_r(\mathbf{x}) = d(\mathbf{x}, A_r) \\ \quad r{=}1,\ldots,M \end{cases} \tag{15}$$

where $d(\mathbf{x}, A_i)$ denotes the Euclidean distance from point $\mathbf{x}$ to point A_i and $\mathbf{x}\in[-10000, 10000]^2$. The ML-DMP has two key characteristics: 1)

its Pareto optimal solutions lie in a regular polygon in the two-dimensional decision space, and 2) these solutions are similar (in the sense of Euclidean geometry) to their images in the high-dimensional objective space. A straightforward understanding of the distribution of the objective vector set can be realized via observing the solution set in the two-dimensional decision space [60].

4.2. Performance Indicators

To make empirical comparison between the results achieved by different algorithms, two widely adopted performance metrics are adopted to assess the qualities of the achieved results.

The first performance indicator applied in this paper is the Inverted Generational Distance (IGD) [61], which can assess both the convergence and distribution of the solution set obtained by MaOEAs. Suppose that P^* is a set of evenly distributed reference points [62] in the PF and Ω is the set of non-dominated solutions found by MaOEAs. The IGD can be mathematically defined as follows.

$$\mathrm{IGD}(P^*, \Omega) = \frac{\sum_{x \in P^*} dis(x, \Omega)}{|P^*|}, \tag{16}$$

where $dis(x, \Omega)$ is the minimum Euclidean distance between x and points in Ω, and $|P^*|$ denotes the number of elements in P^*. The set of reference points required for calculating IGD values are uniformly selected from the PF of each test problem, and a set size closest to 5000 is used in this paper due to the fact that an exact number of 5000 is impossible to be set for each test instance.

The second performance indicator used in this paper is the hypervolume (HV) [63]. Generally, hypervolume is favored because it captures in a single scalar both the closeness of the solutions to the optimal set and, to some extent, the spread of the solutions across objective space. Given a solution set Ω, the HV value of Ω is defined as the area covered by Ω with respect to a set of predefined reference points P^* in the objective space:

$$\mathrm{HV}(\Omega, P^*) = \lambda(H(\Omega, P^*)), \tag{17}$$

where

$$H(\Omega, P^*) = \{z \in Z | \exists x \in P, \exists r \in P^* : f(x) \leq z \leq r\},$$

and λ is the Lebesgue measure with

$$\lambda(H(\Omega, P^*)) = \int_{\mathbb{P}^{*n}} 1_{H(\Omega, P^*)}(z) dz,$$

where $1_{H(\Omega,P^*)}$ is the characteristic function of $H(\Omega, P^*)$.

Note that, a smaller value of IGD will indicate a better performance of the algorithm; in contrast, a greater value of HV will indicate a better performance of the algorithm.

4.3. Experimental Settings

In this subsection, we first present the general parameter settings for the experiments, followed by the specific parameter settings for each compared algorithm.

1) Crossover and Mutation. In the proposed RSEA and all the compared algorithms, the simulated binary crossover [64] and polynomial mutation [65] are adopted to create offspring solutions. The distribution index of crossover is set to $n_c = 20$ and that of mutation is set to $n_m = 20$, as recommended in [66]. The crossover probability $p_c = 1.0$ and the mutation probability $p_m = 1/D$ are used, where D denotes the number of decision variables.

2) Population Size. For MOEA/D, RPD-NSGA-II, and NSGA-III, the population size is determined by the simplex-lattice design factor H together with the objective number m [67]. As recommended in [24], a two-layer reference vector generation strategy is applied for $m > 8$ to generate reference (weight) vectors on both the outer boundaries and inside layers of the Pareto optimal fronts. The details of the settings of the population sizes in MOEA/D, RPD-NSGA-II, and NSGA-III are summarized in Table 3. For the other three algorithms, MaOEA-R&D, PICEA-g, and RSEA, the population sizes are also set according to Table 3 to create a fair environment for comparison.

3) Termination Condition. The maximum number of generations is adopted as the termination criterion for all considered algorithms. For DTLZ1, WFG1,2

Table 3: Setting of population size in NSGA-III, RPD-NSGA-II, and MOEA/D, where p_1 and p_2 are parameters controlling the numbers of weight vectors along the boundary of the Pareto front and inside it, respectively.

Obj.	Parameter(p_1, p_2)	Population size (N)
3	(12,0)	91
5	(4,3)	105
10	(3,1)	230
15	(2,2)	240

and ML-DMP problems, the maximum number of generations is set to 600. For DTLZ3, the maximum number of generations is set to 800, and 700 for MaF2, MaF4, and MaF5. For the other test problems (DTLZ2, DTLZ4 to DTLZ7, and WFG3 to WFG9), the maximum number of generations is set to 500.

4) Specific Parameter Setting in Each Algorithm. The penalty boundary intersection method is adopted in MOEA/D, and the neighborhood size T was specified as 10% of the population size as recommended in [9]. For PICEA-g, the number of preferences $NGloal$ is set to $m \times 100$ as recommended in [27], where m is the number of objectives. It should be highlighted that no specific parameter is involved in RSEA.

4.4. Results on the DTLZ Suite

The statistical results of the IGD and HV values achieved by the seven algorithms over 30 independent runs are summarized in Table 4 and 5, where the best results are highlighted. It can be observed that MOEA/D, NSGA-III, and RSEA have achieved the most best results on these test instances, followed by RPD-NSGA-II. Note that RSEA has achieved the most best results on 15-objective test instances, while MOEA/D and NSGA-III have achieved the best results mainly on 3-, 5-, and 10-objective test instances.

As shown in Fig. 5, MOEA/D and RSEA have achieved the most regularly distributed and well converged solutions on 15-objective DTLZ2, while RPD-NSGA-II fails to obtain a set of well converged solutions, and PICEA-g together

with MaOEA-R&D have obtained solutions which are partially distributed approximating the PF. From the aspect of RadViz, RSEA has achieved the most uniformly distributed results, followed by MOEA/D; while NSGA-III, MaOEA-R&D, RPD-NSGA-II have obtained solutions located partially.

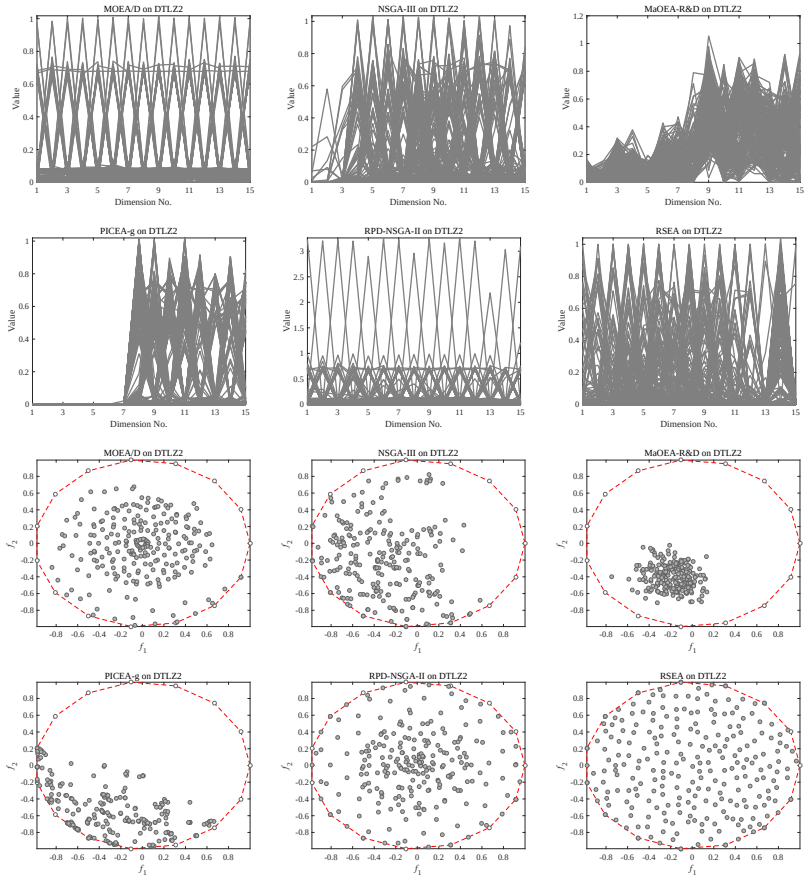

Figure 5: The non-dominated front obtained by each algorithm on DTLZ2 with 15 objectives in the run associated with the median IGD value displayed by parallel coordinates and RadViz, respectively.

DTLZ3 is difficult due to its multimodal property. NSGA-III, RPD-NSGA-II, and RSEA have achieved the best results on 3-, 5-, 10-, and 15-objective instances respectively, while MaOEA-R&D and PICEA-g have not performed well on this problem.

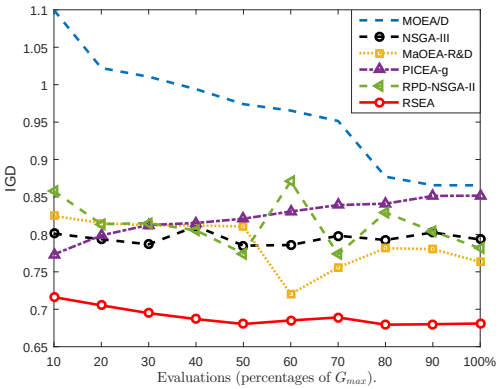

Figure 6: The variations of IGD values achieved by the six compared algorithms on 15-objective DTLZ4.

For DTLZ4, the density of the points on the PF is strongly biased. It can be seen from the table that, RSEA and RPD-NSGA-II have performed well on these test instances, followed by NSGA-III, MaOEA-R&D, PICEA-g, and MOEA/D. The IGD variations achieved by the six compared algorithms on 15-objective DTLZ4 are given in Fig. 6. It is obvious that RSEA has maintained the most stable convergence enhancement over evolution, which has verified the effectiveness of our proposed RSEA on convergence enhancement.

For DTLZ5, 6, and 7, the PFs of these problems are degenerated and discontinuous, which are also known as irregular. The results of HV values and IGD values are not coincident, but the superiority of RSEA and NSGA-III can be verified in comparison with the other four algorithms.

Furthermore, the statistic results of Wilcoxon rank sum test in Table 4 and 5 have shown that all the five compared algorithms have achieved less + (significantly better) results than − (significantly worse) results to that obtained by RSEA. The competitiveness our proposed RSEA in comparison with other five popular algorithms on DTLZ test suites is verified.

Table 4: The IGD Results of MOEA/D, NSGA-III, MaOEA-R&D, PICEA-g, RPD-NSGA-II and RSEA on 28 Test Instances. The Best Result in Each Row is Highlighted.

Problem	Obj.	MOEA/D	NSGA-III	MaOEA-R&D	PICEA-g	RPD-NSGA-II	RSEA
DTLZ1	3	2.00e-2(3.56e-18)≈	2.00e-2(3.56e-18)≈	2.00e-2(3.56e-18)≈	2.38e-1(7.68e-3)−	3.00e-2(1.78e-17)−	2.00e-2(3.56e-18)
	5	8.00e-2(1.42e-17)≈	7.00e-2(2.85e-17)+	8.50e-2(1.15e-2)≈	3.71e-1(3.28e-2)−	8.65e-2(5.87e-3)−	8.15e-2(4.89e-3)
	10	1.67e-1(4.44e-3)≈	1.93e-1(6.12e-2)≈	3.23e-1(8.75e-2)−	4.65e-1(1.36e-2)−	3.00e-1(2.64e-2)−	1.70e-1(2.04e-2)
	15	3.50e-1(1.14e-16)−	3.57e-1(3.14e-2)−	3.47e-1(1.74e-1)−	5.19e-1(2.95e-2)−	3.30e-1(1.79e-2)−	2.45e-1(2.84e-2)
DTLZ2	3	5.00e-2(7.12e-18)≈	5.00e-2(7.12e-18)≈	6.00e-2(3.56e-17)−	1.09e-1(9.68e-3)−	5.95e-2(2.24e-3)−	5.00e-2(7.12e-18)
	5	2.40e-1(1.42e-16)+	2.10e-1(2.85e-17)+	2.62e-1(7.25e-2)−	3.01e-1(1.37e-2)−	2.20e-1(5.70e-17)+	2.51e-1(9.45e-3)
	10	5.20e-1(2.28e-16)≈	5.62e-1(7.82e-2)≈	7.45e-1(3.20e-2)−	8.80e-1(3.09e-2)−	5.25e-1(6.05e-3)≈	5.35e-1(3.43e-2)
	15	1.26e+0(4.59e-2)−	8.13e-1(1.66e-2)−	9.96e-1(5.40e-2)−	1.06e+0(3.40e-2)−	8.24e-1(4.36e-2)−	7.03e-1(2.08e-2)
DTLZ3	3	5.45e-2(5.10e-3)≈	5.30e-2(4.70e-3)≈	6.00e-2(3.56e-17)−	4.49e-1(3.71e-2)−	8.10e-2(4.47e-3)−	5.45e-2(5.10e-3)
	5	2.40e-1(1.42e-16)+	2.10e-1(2.24e-3)+	2.20e-1(7.59e-3)+	7.53e-1(4.53e-2)−	2.91e-1(1.95e-2)−	2.55e-1(6.88e-3)
	10	7.54e-1(2.89e-1)≈	7.44e-1(2.65e-1)−	1.42e+0(1.23e+0)−	1.18e+0(5.84e-2)−	6.13e-1(1.84e-2)+	6.37e-1(4.51e-2)
	15	1.31e+0(2.01e-2)−	9.68e-1(4.71e-2)−	2.59e+0(3.98e+0)−	1.31e+0(2.11e-2)−	1.19e+1(5.27e+0)−	8.84e-1(6.10e-2)
DTLZ4	3	4.67e-1(3.85e-1)−	1.23e-1(1.80e-1)≈	6.00e-2(3.56e-17)−	2.31e-1(2.46e-1)−	6.00e-2(3.56e-17)−	5.00e-2(7.12e-18)
	5	4.96e-1(1.96e-1)−	2.78e-1(1.07e-1)−	3.34e-1(1.01e-1)≈	4.63e-1(1.31e-1)−	2.20e-1(5.70e-17)+	2.73e-1(2.30e-2)
	10	7.01e-1(1.06e-1)−	6.08e-1(9.57e-2)≈	6.06e-1(5.13e-2)−	6.76e-1(7.03e-2)−	5.30e-1(6.86e-3)+	5.35e-1(1.67e-2)
	15	1.09e+0(1.35e-1)−	7.94e-1(2.56e-2)−	7.75e-1(2.91e-2)−	8.61e-1(3.13e-2)−	8.26e-1(1.23e-1)−	6.97e-1(3.85e-2)
DTLZ5	3	3.00e-2(1.78e-17)−	1.10e-2(3.08e-3)≈	7.40e-1(1.14e-16)−	4.05e-2(2.42e-2)−	3.05e-2(2.24e-3)−	1.00e-2(1.78e-18)
	5	5.00e-2(7.12e-18)+	1.12e-1(3.56e-2)−	7.40e-1(1.14e-16)−	7.31e-1(2.79e-2)−	1.40e-1(3.52e-2)−	1.02e-1(1.58e-1)
	10	1.40e-1(5.70e-17)−	3.00e-1(9.94e-2)−	7.40e-1(1.14e-16)−	7.40e-1(1.14e-16)−	2.01e-1(4.82e-2)−	7.45e-2(3.10e-2)
	15	5.20e-1(2.04e-1)−	3.37e-1(1.18e-1)≈	7.40e-1(1.14e-16)−	7.10e-1(5.53e-2)−	3.63e-1(1.26e-1)−	2.86e-1(1.67e-1)
DTLZ6	3	3.00e-2(1.78e-17)+	2.00e-2(3.56e-18)+	7.40e-1(1.14e-16)−	4.13e-1(3.29e-1)−	1.51e-1(6.37e-2)−	3.30e-2(9.39e-2)
	5	5.00e-2(7.12e-18)+	3.36e-1(1.63e-1)−	6.95e-1(1.51e-1)−	3.34e-1(2.02e-1)−	2.96e-1(1.60e-1)−	1.11e-1(8.22e-2)
	10	1.40e-1(5.70e-17)+	1.92e+0(1.16e+0)−	7.40e-1(1.14e-16)−	7.27e-1(3.48e-2)−	2.99e-1(7.66e-2)≈	3.28e-1(1.30e-1)
	15	5.40e-1(2.05e-1)−	4.26e-1(1.47e-1)≈	7.40e-1(1.14e-16)−	7.36e-1(2.01e-2)−	1.31e+0(7.24e-1)−	4.49e-1(1.91e-1)
DTLZ7	3	1.40e-1(5.70e-17)+	7.75e-2(4.44e-3)+	6.53e-1(1.64e-1)−	4.77e-1(3.20e-1)−	1.28e-1(1.61e-1)+	1.50e-1(1.38e-1)
	5	1.07e+0(7.28e-1)−	4.01e-1(2.59e-2)+	2.19e+0(7.08e-1)−	1.94e+0(4.69e-1)−	4.65e-1(1.90e-2)+	5.20e-1(9.14e-2)
	10	3.89e+0(1.64e+0)≈	1.75e+0(2.88e-1)+	4.46e+0(1.60e+0)≈	6.07e+0(9.92e-2)−	1.87e+0(5.40e-1)+	3.58e+0(6.51e-1)
	15	5.32e+0(2.01e+0)+	5.74e+0(5.84e-1)+	2.78e+1(6.35e+0)−	1.17e+1(5.69e-2)−	6.91e+0(1.06e+0)+	9.26e+0(6.70e-1)
+/ − / ≈		8/12/8	8/10/10	1/23/4	0/28/0	8/18/2	

'+', '−' and '≈' indicate that the result is significantly better, significantly worse and statistically similar to that obtained by RSEA, respectively.

Table 5: The HV Results of MOEA/D, NSGA-III, MaOEA-R&D, PICEA-g, RPD-NSGA-II and RSEA on 28 Test Instances. The Best Result in Each Row is Highlighted.

Problem	Obj.	MOEA/D	NSGA-III	MaOEA-R&D	PICEA-g	RPDNSGA-II	RSEA
DTLZ1	3	1.40e-1(5.70e-17)≈	1.40e-1(5.70e-17)≈	1.40e-1(5.70e-17)≈	4.70e-2(6.57e-3)−	1.40e-1(5.70e-17)≈	1.40e-1(5.70e-17)
	5	5.00e-2(7.12e-18)≈	5.00e-2(7.12e-18)≈	5.00e-2(7.12e-18)≈	1.30e-2(5.71e-3)−	5.00e-2(7.12e-18)≈	5.00e-2(7.12e-18)
	10	0.00e+0(0.00e+0)≈	0.00e+0(0.00e+0)≈	0.00e+0(0.00e+0)≈	0.00e+0(0.00e+0)≈	0.00e+0(0.00e+0)≈	0.00e+0(0.00e+0)
	15	0.00e+0(0.00e+0)≈	0.00e+0(0.00e+0)≈	0.00e+0(0.00e+0)≈	0.00e+0(0.00e+0)≈	0.00e+0(0.00e+0)≈	0.00e+0(0.00e+0)
DTLZ2	3	7.40e-1(1.14e-16)≈	7.40e-1(1.14e-16)≈	7.08e-1(5.23e-3)−	7.05e-1(1.36e-2)−	7.40e-1(1.14e-16)≈	7.40e-1(1.14e-16)
	5	1.24e+0(4.56e-16)+	1.25e+0(0.00e+0)+	1.03e+0(3.00e-2)−	1.17e+0(2.99e-2)−	1.24e+0(3.08e-3)+	1.21e+0(5.98e-3)
	10	2.42e+0(4.44e-3)+	2.25e+0(1.79e-1)≈	1.24e+0(2.29e-1)−	1.69e+0(8.12e-2)−	2.38e+0(1.78e-2)+	2.30e+0(2.12e-2)
	15	5.69e-1(1.75e-1)−	2.73e+0(1.27e-1)−	1.42e+0(2.52e-1)−	2.62e+0(2.12e-1)−	1.96e+0(4.24e-1)−	3.77e+0(5.55e-2)
DTLZ3	3	7.34e-1(7.54e-3)−	7.36e-1(6.81e-3)≈	7.14e-1(9.33e-3)−	3.34e-1(2.93e-2)−	7.07e-1(7.16e-3)−	7.39e-1(3.66e-3)
	5	1.23e+0(1.11e-2)+	1.23e+0(1.05e-2)+	1.08e+0(2.39e-2)−	4.20e-1(4.60e-2)−	1.17e+0(2.64e-2)−	1.18e+0(1.06e-2)
	10	1.62e+0(9.87e-1)≈	1.59e+0(7.05e-1)−	7.31e-1(5.19e-1)−	3.56e-1(9.70e-2)−	2.06e+0(7.91e-2)≈	2.02e+0(1.33e-1)
	15	3.97e-1(7.60e-2)−	1.89e+0(2.82e-1)−	1.02e+0(9.40e-1)−	3.59e-1(8.65e-2)−	0.00e+0(0.00e+0)−	2.47e+0(4.95e-1)
DTLZ4	3	4.67e-1(2.64e-1)−	6.97e-1(1.06e-1)−	7.16e-1(5.10e-3)−	6.29e-1(1.61e-1)−	7.40e-1(1.14e-16)≈	7.41e-1(3.08e-3)
	5	9.97e-1(2.45e-1)−	1.19e+0(8.92e-2)−	1.05e+0(4.83e-2)−	1.05e+0(1.31e-1)−	1.24e+0(5.71e-3)+	1.21e+0(1.06e-2)
	10	2.06e+0(3.17e-1)−	2.17e+0(2.20e-1)≈	1.83e+0(1.05e-1)−	2.15e+0(1.34e-1)−	2.40e+0(6.41e-3)+	2.33e+0(2.88e-2)
	15	1.37e+0(6.54e-1)−	3.14e+0(1.60e-1)−	3.00e+0(1.61e-1)−	3.50e+0(1.12e-1)−	1.63e+0(5.04e-1)−	3.87e+0(7.68e-2)
DTLZ5	3	1.20e-1(7.12e-17)−	1.30e-1(5.70e-17)≈	6.00e-2(3.56e-17)−	1.28e-1(3.66e-3)≈	1.20e-1(7.12e-17)−	1.30e-1(5.70e-17)
	5	1.00e-2(1.78e-18)≈	1.00e-2(1.78e-18)≈	1.00e-2(1.78e-18)≈	1.00e-2(1.78e-18)≈	1.00e-2(1.78e-18)≈	1.00e-2(1.78e-18)
	10	0.00e+0(0.00e+0)≈	0.00e+0(0.00e+0)≈	0.00e+0(0.00e+0)≈	0.00e+0(0.00e+0)≈	0.00e+0(0.00e+0)≈	0.00e+0(0.00e+0)
	15	0.00e+0(0.00e+0)≈	0.00e+0(0.00e+0)≈	0.00e+0(0.00e+0)≈	0.00e+0(0.00e+0)≈	0.00e+0(0.00e+0)≈	0.00e+0(0.00e+0)
DTLZ6	3	1.20e-1(7.12e-17)−	1.30e-1(5.70e-17)≈	6.00e-2(3.56e-17)−	8.20e-2(2.35e-2)−	9.75e-2(1.16e-2)−	1.30e-1(5.70e-17)
	5	1.00e-2(1.78e-18)≈	9.00e-3(3.08e-3)≈	9.50e-3(2.24e-3)≈	1.00e-2(1.78e-18)≈	9.00e-3(3.08e-3)≈	1.00e-2(1.78e-18)
	10	0.00e+0(0.00e+0)≈	0.00e+0(0.00e+0)≈	0.00e+0(0.00e+0)≈	0.00e+0(0.00e+0)≈	0.00e+0(0.00e+0)≈	0.00e+0(0.00e+0)
	15	0.00e+0(0.00e+0)≈	0.00e+0(0.00e+0)≈	0.00e+0(0.00e+0)≈	0.00e+0(0.00e+0)≈	0.00e+0(0.00e+0)≈	0.00e+0(0.00e+0)
DTLZ7	3	1.51e+0(7.45e-3)−	1.61e+0(5.23e-3)+	1.16e+0(1.26e-1)−	1.35e+0(2.06e-1)−	1.57e+0(9.18e-2)−	1.61e+0(7.98e-2)
	5	8.57e-1(4.68e-1)−	2.06e+0(2.90e-2)−	1.22e+0(2.57e-1)−	1.41e+0(1.66e-1)−	2.04e+0(1.17e-2)−	2.18e+0(7.68e-2)
	10	3.00e-3(9.23e-3)−	2.09e+0(1.38e-1)−	4.10e-2(4.81e-2)−	1.47e+0(4.43e-2)−	2.02e+0(9.61e-2)−	2.19e+0(7.44e-2)
	15	0.00e+0(0.00e+0)−	8.10e-1(1.66e-1)−	0.00e+0(0.00e+0)−	1.52e+0(2.50e-2)−	1.75e+0(1.27e-1)−	2.11e+0(3.94e-2)
+/ − / ≈		3/13/12	3/9/16	0/18/10	0/19/9	4/11/13	

'+', '−' and '≈' indicate that the result is significantly better, significantly worse and statistically similar to that obtained by RSEA, respectively.

4.5. Results on the WFG Suite

The statistical results of the HV values achieved by the six algorithms over 30 independent runs are displayed in Table 6 and 7. It can be observed that RSEA achieved the most best results on 36 test instances, and RSEA together with RPD-NSGA-II and NSGA-III have shown to be overall outperforming the other three compared algorithms. In what follows, some discussions on the experimental results are given.

WFG1, 2, and 3 are designed with irregular PFs. RSEA has achieved the most best results, which demonstrates the competitive performance of the proposed RSEA compared with the other five algorithms. Fig. 7 displays the non-dominated solutions obtained by the six compared algorithms on 15-objective WFG1 in the run associated with the median HV value, and RSEA has achieved the best result with the obtained non-dominated solutions evenly distributed, followed by RPD-NSGA-II and NSGA-III. The solutions obtained by MOEA/D, MaOEA-R&D, and PICEA-g are distributed around the partial region of the PF. Similar results can be observed on RadViz.

WFG4 to WFG9 are designed with the difficulties in decision space, e.g., multimodality for WFG4, landscape deception of WFG5 and non-separability for WFG6, 8, and 9, though their PFs are of the same convex structure. It can be observed from Table 7, RSEA and RPD-NSGA-II show the most competitive overall performance on these six problems by achieving the best results on 20 out of 24 instances. Note that RSEA achieves the most best results on 3- and 15-objective problems while RPD-NSGA-II mainly achieves the best results on 5- and 10-objective problems.

The variations of HV values on 15-objective WFG4 is given in Fig. 8. It is obvious that RSEA has performed the best in comparison with other five algorithms on convergence enhancement and diversity maintenance on WFG4.

To summarize, we can conclude from Table 6, 7, and Fig 7 that RSEA performs the best among the five compared algorithms.

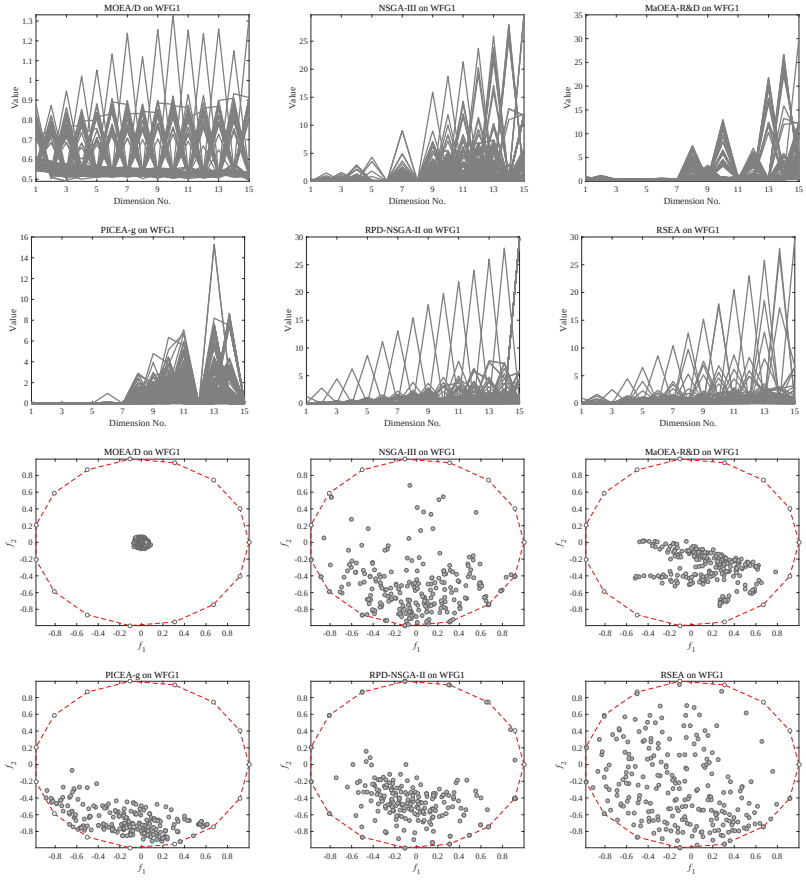

Figure 7: The non-dominated front obtained by each algorithm on WFG1 with 15 objectives in the run associated with the median HV value are displayed by parallel coordinates and RadViz, respectively.

Table 6: The IGD Results of MOEA/D, NSGA-III, MaOEA-R&D, PICEA-g, RPD-NSGA-II and RSEA on 36 Test Instances. The Best Result in Each Row is Highlighted.

Problem	Obj.	MOEA/D	NSGA-III	MaOEA-R&D	PICEA-g	RPD-NSGA-II	RSEA
WFG1	3	3.36e-1(2.30e-2)−	1.63e-1(1.79e-2)+	4.02e-1(6.60e-2)−	2.61e-1(4.01e-2)−	4.61e-1(3.34e-1)−	1.80e-1(2.38e-2)
	5	1.54e+0(1.01e-1)−	4.93e-1(1.98e-2)+	1.49e+0(2.58e-1)−	1.83e+0(6.86e-1)−	6.69e-1(1.00e-1)−	5.49e-1(1.77e-2)
	10	3.33e+0(8.62e-2)−	2.29e+0(7.33e-1)≈	2.73e+0(5.92e-1)−	3.21e+0(1.18e-1)−	2.09e+0(4.60e-1)≈	1.97e+0(2.87e-1)
	15	5.10e+0(9.68e-2)−	4.51e+0(4.77e-1)−	4.58e+0(1.06e+0)−	4.81e+0(1.37e-1)−	4.49e+0(3.61e-1)−	3.50e+0(2.61e-1)
WFG2	3	8.65e-1(1.14e-1)−	1.96e-1(6.05e-3)+	1.76e-1(8.21e-3)+	4.65e-1(1.24e-1)−	2.08e-1(2.81e-2)+	2.24e-1(2.19e-2)
	5	4.78e+0(2.08e-1)−	9.64e-1(2.52e-2)−	8.23e-1(2.67e-1)≈	2.36e+0(3.24e-1)−	1.07e+0(1.40e-1)−	7.93e-1(6.60e-2)
	10	1.21e+1(8.86e-2)−	3.98e+0(1.25e+0)−	1.68e+0(1.94e-1)+	6.94e+0(1.26e+0)−	3.18e+0(1.42e+0)−	2.02e+0(1.35e-1)
	15	1.59e+1(2.24e-3)−	8.05e+0(2.36e+0)≈	1.03e+1(8.26e-1)−	1.53e+1(3.78e-1)−	1.84e-1(3.12e-1)+	8.05e+0(1.38e+0)
WFG3	3	1.62e-1(1.23e-2)−	1.12e-1(1.23e-2)−	3.18e+0(1.23e-2)−	3.68e-1(2.54e-1)−	1.53e-1(1.30e-2)−	9.90e-2(9.94e-2)
	5	8.77e-1(6.43e-2)−	5.95e-1(4.52e-2)−	2.59e+0(1.68e+0)−	4.17e+0(2.31e-1)−	6.58e-1(6.65e-2)−	2.27e-1(1.59e-1)
	10	9.57e+0(2.34e-1)−	2.99e+0(8.88e-1)≈	4.80e+0(9.05e-1)−	9.96e+0(5.33e-1)−	2.10e+0(4.76e-2)+	3.67e+0(1.51e+0)
	15	1.80e+1(0.00e+0)−	4.28e+0(7.86e-1)+	6.49e+0(9.95e-1)+	1.58e+1(7.80e-1)−	7.31e+0(1.36e+0)+	1.07e+1(1.31e+0)
WFG4	3	2.45e-1(5.13e-3)−	2.20e-1(5.70e-17)−	2.62e-1(1.82e-2)−	3.49e-1(2.46e-2)−	2.34e-1(6.71e-3)−	2.16e-1(5.10e-3)
	5	2.13e+0(2.27e-1)−	1.23e+0(4.44e-3)+	1.32e+0(5.55e-2)+	1.60e+0(5.73e-2)−	1.32e+0(3.86e-2)+	1.40e+0(2.70e-2)
	10	9.70e+0(5.63e-1)−	5.71e+0(1.69e-1)−	6.53e+0(4.30e-1)−	1.01e+1(1.63e+0)−	5.90e+0(8.37e-2)−	5.36e+0(1.55e-1)
	15	1.75e+1(4.77e-2)−	1.21e+1(2.79e-1)−	1.45e+1(1.17e+0)−	2.20e+1(1.71e+0)−	1.24e+1(2.32e-1)−	1.03e+1(4.05e-1)
WFG5	3	2.44e-1(5.03e-3)−	2.30e-1(5.70e-17)−	2.59e-1(8.52e-3)−	3.84e-1(2.80e-2)−	2.37e-1(6.57e-3)−	2.28e-1(4.10e-3)
	5	1.96e+0(1.46e-1)−	1.22e+0(2.28e-16)+	1.30e+0(4.97e-2)+	1.62e+0(6.47e-2)−	1.28e+0(3.59e-2)+	1.37e+0(3.77e-2)
	10	9.35e+0(2.95e-1)−	5.60e+0(6.05e-3)−	6.46e+0(4.03e-1)−	1.06e+1(1.23e+0)−	5.85e+0(5.84e-2)−	5.27e+0(1.98e-1)
	15	1.74e+1(6.69e-2)−	1.21e+1(1.60e-1)−	1.35e+1(7.65e-1)−	2.24e+1(9.28e-1)−	1.23e+1(1.43e-1)−	1.06e+1(6.29e-1)
WFG6	3	2.72e-1(1.01e-2)−	2.43e-1(1.13e-2)−	2.87e-1(4.33e-2)−	4.08e-1(2.65e-2)−	2.54e-1(1.43e-2)−	2.35e-1(1.05e-2)
	5	2.70e+0(9.57e-2)−	1.22e+0(2.24e-3)+	1.42e+0(3.75e-2)−	1.70e+0(7.56e-2)−	1.29e+0(2.34e-2)+	1.39e+0(3.08e-2)
	10	1.06e+1(2.34e-1)−	6.75e+0(1.11e+0)−	6.19e+0(4.10e-1)−	8.97e+0(9.08e-1)−	5.84e+0(6.17e-2)−	5.39e+0(1.83e-1)
	15	1.75e+1(5.11e-2)−	1.25e+1(7.09e-1)−	1.40e+1(1.08e+0)−	1.96e+1(1.25e+0)−	1.24e+1(1.56e-1)−	1.09e+1(8.46e-1)
WFG7	3	2.73e-1(1.26e-2)−	2.20e-1(5.70e-17)−	2.77e-1(1.08e-2)−	4.52e-1(3.38e-2)−	2.31e-1(5.53e-3)−	2.15e-1(5.13e-3)
	5	2.79e+0(1.16e-1)−	1.23e+0(2.28e-16)+	1.42e+0(5.21e-2)≈	1.76e+0(8.15e-2)−	1.29e+0(1.95e-2)+	1.44e+0(6.07e-2)
	10	1.06e+1(6.05e-3)−	5.71e+0(9.03e-2)−	6.53e+0(3.77e-1)−	7.47e+0(1.23e+0)−	5.91e+0(8.46e-2)−	5.38e+0(1.47e-1)
	15	1.75e+1(6.20e-2)−	1.18e+1(3.75e-1)−	1.65e+1(9.73e-1)−	1.87e+1(2.18e+0)−	1.21e+1(2.93e-1)−	1.04e+1(1.16e+0)
WFG8	3	3.02e-1(6.16e-3)−	2.88e-1(4.10e-3)≈	3.46e-1(1.05e-2)−	5.42e-1(8.51e-2)−	3.08e-1(5.23e-3)−	2.87e-1(4.89e-3)
	5	2.10e+0(4.00e-1)−	1.26e+0(1.23e-2)+	1.60e+0(7.98e-2)−	1.73e+0(7.67e-2)−	1.27e+0(1.88e-2)+	1.41e+0(2.69e-2)
	10	8.94e+0(1.47e+0)−	6.33e+0(5.44e-1)+	7.09e+0(5.25e-1)−	8.92e+0(1.27e+0)−	5.77e+0(3.84e-2)+	6.64e+0(2.78e-1)
	15	1.48e+1(8.47e-1)−	1.33e+1(6.40e-1)−	1.59e+1(6.85e-1)−	1.83e+1(1.86e+0)−	1.26e+1(6.41e-2)≈	1.26e+1(4.80e-1)
WFG9	3	2.67e-1(2.57e-2)−	2.35e-1(3.94e-2)−	2.59e-1(1.31e-2)−	3.80e-1(3.26e-2)−	2.60e-1(4.52e-2)−	2.16e-1(5.03e-3)
	5	2.11e+0(2.24e-1)−	1.21e+0(1.19e-2)+	1.40e+0(7.52e-2)≈	1.58e+0(7.44e-2)−	1.41e+0(3.53e-1)−	1.36e+0(5.42e-2)
	10	9.45e+0(8.84e-1)−	5.63e+0(1.18e-1)−	6.80e+0(4.22e-1)−	9.97e+0(8.70e-1)−	6.35e+0(8.30e-1)−	5.36e+0(1.74e-1)
	15	1.57e+1(1.82e+0)−	1.18e+1(2.65e-1)−	1.43e+1(6.17e-1)−	2.33e+1(1.97e+0)−	1.25e+1(1.34e-1)−	1.07e+1(5.79e-1)
+/ − / ≈		0/36/0	11/21/4	5/28/3	0/36/0	10/24/2	

'+', '−' and '≈' indicate that the result is significantly better, significantly worse and statistically similar to that obtained by RSEA, respectively.

Table 7: The HV Results of MOEA/D, NSGA-III, MaOEA-R&D, PICEA-g, RPD-NSGA-II and RSEA on 36 Test Instances. The Best Result in Each Row is Highlighted.

Problem	Obj.	MOEA/D	NSGA-III	MaOEA-R&D	PICEA-g	RPD-NSGA-II	RSEA
WFG1	3	5.54e+1(1.76e+0)−	5.96e+1(8.78e-1)−	5.16e+1(2.58e+0)−	5.92e+1(7.81e-1)−	5.57e+1(6.92e+0)−	6.01e+1(1.52e-1)
	5	5.71e+3(7.36e+1)−	6.08e+3(1.21e+2)≈	2.86e+3(5.40e+2)−	6.13e+3(1.58e+1)−	6.12e+3(4.37e+1)−	6.15e+3(2.87e+0)
	10	4.56e+9(8.52e+8)−	9.58e+9(1.05e+8)≈	3.73e+9(1.81e+9)−	9.41e+9(4.50e+8)−	9.48e+9(3.57e+8)−	9.64e+9(9.22e+5)
	15	6.17e+16(1.27e+16)−	1.77e+17(1.08e+15)−	1.04e+17(3.14e+16)−	1.70e+17(1.13e+16)−	1.76e+17(1.72e+15)−	1.78e+17(3.39e+15)
WFG2	3	5.81e+1(3.39e-1)−	5.94e+1(6.22e-2)−	5.87e+1(1.10e-1)−	5.91e+1(2.58e-1)−	5.97e+1(4.89e-2)+	5.95e+1(9.80e-2)
	5	5.89e+3(2.23e+1)−	6.15e+3(5.70e+0)+	5.88e+3(4.43e+1)−	5.78e+3(2.76e+1)−	6.14e+3(1.06e+1)+	6.12e+3(6.00e+0)
	10	8.77e+9(5.14e+7)−	9.54e+9(8.56e+7)−	9.33e+9(2.21e+8)−	9.12e+9(1.31e+8)−	9.45e+9(1.78e+8)−	9.62e+9(3.88e+6)
	15	1.62e+17(5.81e+14)−	1.75e+17(2.44e+15)−	1.70e+17(1.19e+15)−	1.64e+17(4.67e+15)−	1.76e+17(1.93e+15)−	1.78e+17(2.92e+14)
WFG3	3	5.77e+0(9.70e-2)−	6.14e+0(7.53e-2)−	1.48e+0(2.67e-2)−	6.23e+0(2.32e-1)−	5.88e+0(8.75e-2)−	6.38e+0(3.65e-2)
	5	1.17e+0(4.19e-1)−	2.12e+0(2.40e-1)−	2.83e-1(5.02e-1)−	2.14e+0(1.51e-1)−	1.84e+0(6.62e-2)−	3.21e+0(3.73e-2)
	10	0.00e+0(0.00e+0)≈	0.00e+0(0.00e+0)≈	0.00e+0(0.00e+0)≈	0.00e+0(0.00e+0)≈	0.00e+0(0.00e+0)≈	0.00e+0(0.00e+0)
	15	0.00e+0(0.00e+0)≈	0.00e+0(0.00e+0)≈	0.00e+0(0.00e+0)≈	0.00e+0(0.00e+0)≈	0.00e+0(0.00e+0)≈	0.00e+0(0.00e+0)
WFG4	3	3.44e+1(1.09e-1)−	3.55e+1(4.83e-2)−	3.20e+1(5.86e-1)−	3.47e+1(2.10e-1)−	3.55e+1(8.42e-2)−	3.56e+1(2.68e-2)
	5	3.91e+3(2.27e+2)−	4.74e+3(1.09e+1)+	3.44e+3(1.72e+2)−	4.66e+3(3.56e+1)+	4.75e+3(1.66e+1)+	4.61e+3(2.73e+1)
	10	3.17e+9(1.04e+9)−	8.81e+9(5.66e+8)+	5.46e+9(1.70e+9)−	6.13e+9(8.04e+8)−	9.04e+9(1.79e+7)+	8.44e+9(2.20e+8)
	15	4.30e+16(7.19e+15)−	1.23e+17(8.24e+15)−	1.09e+17(2.22e+16)−	9.92e+16(1.32e+16)−	1.43e+17(1.51e+15)−	1.61e+17(3.40e+15)
WFG5	3	3.20e+1(2.87e-1)−	3.31e+1(8.13e-3)+	3.03e+1(1.35e-1)−	3.18e+1(3.15e-1)−	3.30e+1(9.55e-2)−	3.30e+1(4.59e-2)
	5	3.81e+3(1.10e+2)−	4.47e+3(3.75e+0)+	3.33e+3(1.21e+2)−	4.32e+3(3.45e+1)+	4.46e+3(1.68e+1)+	4.30e+3(2.90e+1)
	10	3.08e+9(5.19e+8)−	8.43e+9(2.77e+6)+	3.46e+9(4.45e+8)−	5.22e+9(6.22e+8)−	8.43e+9(1.10e+7)+	7.91e+9(1.72e+8)
	15	3.69e+16(9.08e+15)−	1.19e+17(1.12e+16)−	6.53e+16(1.44e+16)−	8.27e+16(6.28e+15)−	1.24e+17(3.29e+15)−	1.47e+17(4.82e+15)
WFG6	3	3.09e+1(8.86e-1)−	3.21e+1(8.62e-1)≈	3.06e+1(1.37e+0)−	3.09e+1(7.64e-1)−	3.17e+1(1.27e+0)−	3.29e+1(1.12e+0)
	5	2.66e+3(2.33e+2)−	4.34e+3(9.37e+1)+	2.93e+3(1.73e+2)−	4.20e+3(1.32e+2)≈	4.35e+3(9.90e+1)+	4.24e+3(9.48e+1)
	10	1.05e+9(2.68e+8)−	6.81e+9(1.24e+9)≈	4.70e+9(1.40e+9)−	6.07e+9(4.18e+8)−	8.29e+9(2.55e+8)+	7.85e+9(1.61e+8)
	15	1.21e+16(5.47e+15)−	1.06e+17(8.47e+15)−	8.06e+16(2.15e+16)−	1.03e+17(7.60e+15)−	1.20e+17(8.21e+15)−	1.43e+17(5.97e+15)
WFG7	3	3.32e+1(4.98e-1)−	3.55e+1(3.72e-2)−	3.17e+1(3.37e-1)−	3.37e+1(2.82e-1)−	3.54e+1(6.97e-2)−	3.57e+1(2.11e-2)
	5	3.05e+3(2.62e+2)−	4.75e+3(9.02e+0)+	3.11e+3(7.85e+1)−	4.59e+3(3.70e+1)≈	4.76e+3(1.25e+1)+	4.61e+3(3.39e+1)
	10	1.56e+9(6.66e+7)−	8.85e+9(5.53e+8)+	2.74e+9(4.94e+8)−	7.41e+9(6.05e+8)−	9.01e+9(5.10e+7)+	8.58e+9(1.60e+8)
	15	2.64e+16(1.14e+16)−	1.25e+17(6.75e+15)−	3.05e+16(6.11e+15)−	1.22e+17(1.32e+16)−	1.42e+17(3.99e+15)−	1.63e+17(5.18e+15)
WFG8	3	2.93e+1(2.34e-1)−	2.99e+1(1.33e-1)≈	2.83e+1(1.88e-1)−	2.69e+1(1.02e+0)−	2.93e+1(1.72e-1)−	2.99e+1(1.13e-1)
	5	2.53e+3(9.56e+2)−	3.99e+3(2.34e+1)+	2.96e+3(2.87e+2)−	3.78e+3(7.16e+1)−	4.03e+3(2.17e+1)+	3.83e+3(6.24e+1)
	10	1.54e+9(2.88e+9)−	6.79e+9(7.78e+8)≈	4.42e+9(1.02e+9)−	6.66e+9(6.28e+8)−	7.89e+9(5.81e+7)+	7.15e+9(1.21e+8)
	15	8.50e+16(2.15e+16)−	9.64e+16(6.43e+15)−	8.41e+16(2.12e+16)−	1.22e+17(1.06e+16)−	1.05e+17(1.19e+15)−	1.34e+17(3.87e+15)
WFG9	3	3.08e+1(1.55e+0)−	3.32e+1(2.45e+0)−	3.09e+1(5.73e-1)−	3.32e+1(3.78e-1)−	3.27e+1(1.87e+0)−	3.47e+1(2.56e-1)
	5	3.08e+3(6.03e+2)−	4.21e+3(2.92e+2)−	3.03e+3(1.70e+2)−	4.52e+3(6.26e+1)+	4.09e+3(4.41e+2)−	4.39e+3(3.34e+1)
	10	2.06e+9(1.39e+9)−	7.16e+9(7.76e+8)−	2.75e+9(9.43e+8)−	5.84e+9(4.29e+8)−	6.02e+9(1.40e+9)−	7.94e+9(1.33e+8)
	15	4.88e+16(3.04e+16)−	1.07e+17(1.42e+16)−	5.88e+16(1.21e+16)−	8.38e+16(1.53e+16)−	6.33e+16(1.55e+16)−	1.50e+17(2.60e+15)
+/ − / ≈		0/34/2	10/18/8	0/34/2	3/29/4	12/22/2	

'+', '−' and '≈' indicate that the result is significantly better, significantly worse and statistically similar to that obtained by RSEA, respectively.

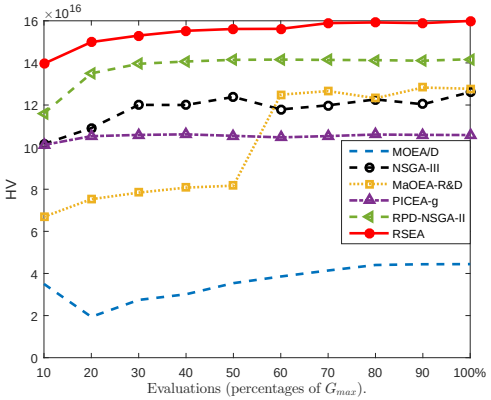

Figure 8: The variations of HV values achieved by the six compared algorithms on 15-objective WFG4.

4.6. Results on the MaF and ML-DMP

In this part, MaF2, 4, 5 and ML-DMP are used to verify the diversity maintenance of our proposed RSEA in comparison with five popular MaOEAs. The IGD and HV results obtained by the six compared algorithms are displayed in Table 8 and 9, and RSEA has achieved the most best results, followed by RPD-NSGA-II.

For MaF2, 4, and 5, the main difficulties of these problems are the biased and badly scaled PFs. It can be observed from Table 9 that RSEA showed the most competitive performance on these MaF test problems.

In Fig. 9, the non-dominated front obtained by each algorithm on ML-DMP with 15 objectives in the run associated with the median HV value is displayed by parallel coordinates and RadViz, and the obtained decision vectors of each algorithm are displayed. Since the Pareto optimal solutions are similar to their image in the objective space, distribution of solutions in decision space can reflect that of the solutions in objective space. It is obvious that RSEA has achieved the best result on this problem, while the other algorithms can only achieve overlapped solutions.

To summarize, our proposed RSEA is effective on diversity maintenance for many-objective optimization.

Table 8: The IGD Results of MOEA/D, NSGA-III, MaOEA-R&D, PICEA-g, RPD-NSGA-II and RSEA on 16 Test Instances. The Best Result in Each Row is Highlighted.

Problem	Obj.	MOEA/D	NSGA-III	MaOEA-R&D	PICEA-g	RPD-NSGA-II	RSEA
MaF2	3	4.00e-2(7.12e-18)−	4.00e-2(7.12e-18)−	1.97e-1(8.69e-2)−	6.15e-2(5.87e-3)−	4.00e-2(7.12e-18)−	3.00e-2(1.78e-17)
	5	1.50e-1(2.85e-17)−	1.40e-1(3.24e-3)−	4.88e-1(3.21e-2)−	1.71e-1(4.47e-3)−	1.41e-1(2.24e-3)−	1.33e-1(5.87e-3)
	10	4.50e-1(2.24e-3)−	2.85e-1(5.31e-2)+	8.39e-1(2.43e-2)−	8.51e-1(1.04e-2)−	2.26e-1(7.59e-3)+	3.67e-1(2.23e-2)
	15	7.60e-1(4.15e-2)−	3.26e-1(4.67e-2)+	8.79e-1(1.79e-2)−	8.94e-1(5.98e-3)−	2.31e-1(4.47e-3)+	4.39e-1(1.66e-1)
MaF4	3	7.76e-1(7.86e-2)−	3.45e-1(1.24e-2)≈	2.89e+0(2.20e-1)−	1.80e+0(2.07e-1)−	4.27e-1(3.66e-2)−	3.67e-1(5.98e-2)
	5	9.61e+0(5.15e-1)−	3.73e+0(4.34e-1)−	1.44e+1(1.59e+0)−	6.51e+0(1.41e+0)−	4.64e+0(5.19e-1)−	3.07e+0(1.85e-1)
	10	4.64e+2(3.85e+0)−	1.73e+2(4.06e+1)−	5.10e+2(8.27e+1)−	1.23e+2(2.45e+1)+	1.91e+2(3.47e+1)−	1.38e+2(1.72e+1)
	15	1.74e+4(3.56e+1)−	5.98e+3(2.33e+2)−	1.53e+4(4.51e+3)−	2.69e+3(6.15e+2)+	7.94e+3(2.02e+3)−	5.35e+3(4.27e+2)
MaF5	3	2.29e+0(2.06e+0)−	5.08e-1(5.09e-1)−	2.71e-1(3.66e-3)−	7.23e-1(4.67e-1)−	2.67e-1(5.50e-3)−	2.45e-1(5.13e-3)
	5	8.90e+0(1.91e+0)−	2.79e+0(1.15e+0)−	3.08e+0(1.57e+0)−	4.58e+0(1.86e+0)−	2.43e+0(4.47e-2)+	2.53e+0(1.16e-1)
	10	2.95e+2(9.36e-1)−	1.29e+2(8.22e-1)−	8.09e+1(2.84e+1)≈	9.71e+1(2.83e+1)≈	9.87e+1(8.69e+0)−	8.32e+1(1.24e+1)
	15	6.72e+3(1.42e-2)−	4.38e+3(5.43e+2)−	1.84e+3(6.68e+2)+	2.27e+3(6.07e+2)≈	4.07e+3(9.35e+2)−	2.55e+3(4.06e+2)
ML-DMP	3	1.16e-1(1.05e-2)−	1.12e-1(4.10e-3)−	3.34e-1(7.53e-2)−	5.14e-1(7.53e-2)−	4.54e-1(4.02e-1)−	7.35e-2(7.45e-3)
	5	3.16e-1(1.54e-2)−	2.60e-1(2.05e-2)−	9.70e-1(8.34e-2)−	6.50e-1(7.73e-2)−	3.76e-1(3.47e-2)−	1.52e-1(1.35e-2)
	10	1.12e+0(6.49e-3)−	5.18e-1(6.66e-2)−	1.61e+0(1.50e-1)−	9.43e-1(9.23e-2)−	6.56e-1(7.64e-2)−	2.41e-1(2.25e-2)
	15	1.59e+0(2.19e-2)−	8.34e-1(9.30e-2)−	1.89e+0(7.17e-2)−	1.07e+0(8.55e-2)−	1.08e+0(1.03e-1)−	2.91e-1(3.63e-2)
+/ − / ≈		0/16/0	2/13/1	1/14/1	2/12/2	3/13/0	

'+', '−' and '≈' indicate that the result is significantly better, significantly worse and statistically similar to that obtained by RSEA, respectively.

Table 9: The HV Results of MOEA/D, NSGA-III, MaOEA-R&D, PICEA-g, RPD-NSGA-II and RSEA on 16 Test Instances. The Best Result in Each Row is Highlighted.

Problem	Obj.	MOEA/D	NSGA-III	MaOEA-R&D	PICEA-g	RPD-NSGA-II	RSEA
MaF2	3	2.10e-1(2.85e-17)−	2.10e-1(2.85e-17)−	1.05e-1(4.91e-2)−	1.99e-1(3.66e-3)−	2.10e-1(2.85e-17)−	2.20e-1(5.70e-17)
	5	4.00e-2(7.12e-18)−	4.00e-2(7.12e-18)−	1.00e-2(1.78e-18)−	4.80e-2(4.10e-3)−	4.00e-2(7.12e-18)−	5.00e-2(7.12e-18)
	10	1.00e-2(1.78e-18)≈	1.00e-2(1.78e-18)≈	0.00e+0(0.00e+0)−	0.00e+0(0.00e+0)−	1.00e-2(1.78e-18)≈	1.00e-2(1.78e-18)
	15	0.00e+0(0.00e+0)≈	0.00e+0(0.00e+0)≈	0.00e+0(0.00e+0)≈	0.00e+0(0.00e+0)≈	0.00e+0(0.00e+0)≈	0.00e+0(0.00e+0)
MaF4	3	4.19e+1(5.86e-1)−	4.35e+1(4.43e-1)−	1.75e+1(2.15e+0)−	7.21e+0(2.25e+0)−	4.26e+1(6.30e-1)−	4.50e+1(4.33e-1)
	5	6.66e+2(1.31e+2)−	2.70e+3(4.97e+2)−	6.88e+2(2.28e+2)−	3.71e+2(1.86e+2)−	3.60e+3(3.29e+2)−	5.29e+3(9.01e+1)
	10	3.77e+9(3.91e+8)−	1.53e+13(1.44e+12)−	4.13e+12(6.16e+12)−	1.07e+11(7.21e+10)−	3.40e+12(2.56e+12)−	2.63e+13(7.32e+11)
	15	8.67e+23(4.66e+22)−	5.61e+29(6.93e+28)−	1.51e+29(1.99e+29)−	0.00e+0(0.00e+0)−	1.10e+25(1.14e+25)−	1.59e+30(1.06e+29)
MaF5	3	2.82e+1(1.72e+1)−	4.39e+1(7.65e+0)≈	4.58e+1(2.14e-1)−	4.14e+1(7.57e+0)−	4.74e+1(9.96e-2)−	4.76e+1(3.76e-2)
	5	2.33e+4(4.21e+3)−	3.95e+4(2.93e+3)−	3.48e+4(3.07e+3)−	3.47e+4(5.90e+3)−	4.05e+4(1.32e+2)+	4.00e+4(2.62e+2)
	10	1.98e+16(9.81e+15)−	8.78e+16(3.04e+13)+	6.29e+16(3.48e+15)−	7.79e+16(4.55e+15)−	8.65e+16(4.19e+14)+	8.35e+16(1.52e+15)
	15	8.87e+35(3.29e+35)−	4.39e+36(1.73e+35)−	3.84e+36(3.88e+35)−	4.63e+36(1.18e+35)−	2.14e+36(8.24e+35)−	5.15e+36(8.19e+34)
ML-DMP	3	1.74e+0(2.87e-2)−	1.75e+0(2.28e-2)−	1.27e+0(1.57e-1)−	8.48e-1(1.12e-1)−	1.03e+0(7.70e-1)−	1.86e+0(2.38e-2)
	5	3.93e+0(5.05e-2)−	3.57e+0(2.35e-1)−	1.29e+0(2.93e-1)−	1.39e+0(4.62e-1)−	3.08e+0(3.46e-1)−	4.56e+0(4.22e-2)
	10	1.23e+1(1.68e-1)−	1.46e+1(2.33e+0)−	2.93e+0(1.69e+0)−	1.37e+0(2.04e+0)−	1.07e+1(1.02e+0)−	2.48e+1(1.20e-1)
	15	2.20e+1(1.15e+0)−	2.35e+1(4.31e+0)−	6.68e+0(2.40e+0)−	2.29e-1(1.31e-1)−	1.38e+1(3.08e+0)−	6.81e+1(1.19e+0)
+/ − / ≈		0/14/2	1/12/3	0/15/1	0/15/1	2/12/2	

'+', '−' and '≈' indicate that the result is significantly better, significantly worse and statistically similar to that obtained by RSEA, respectively.

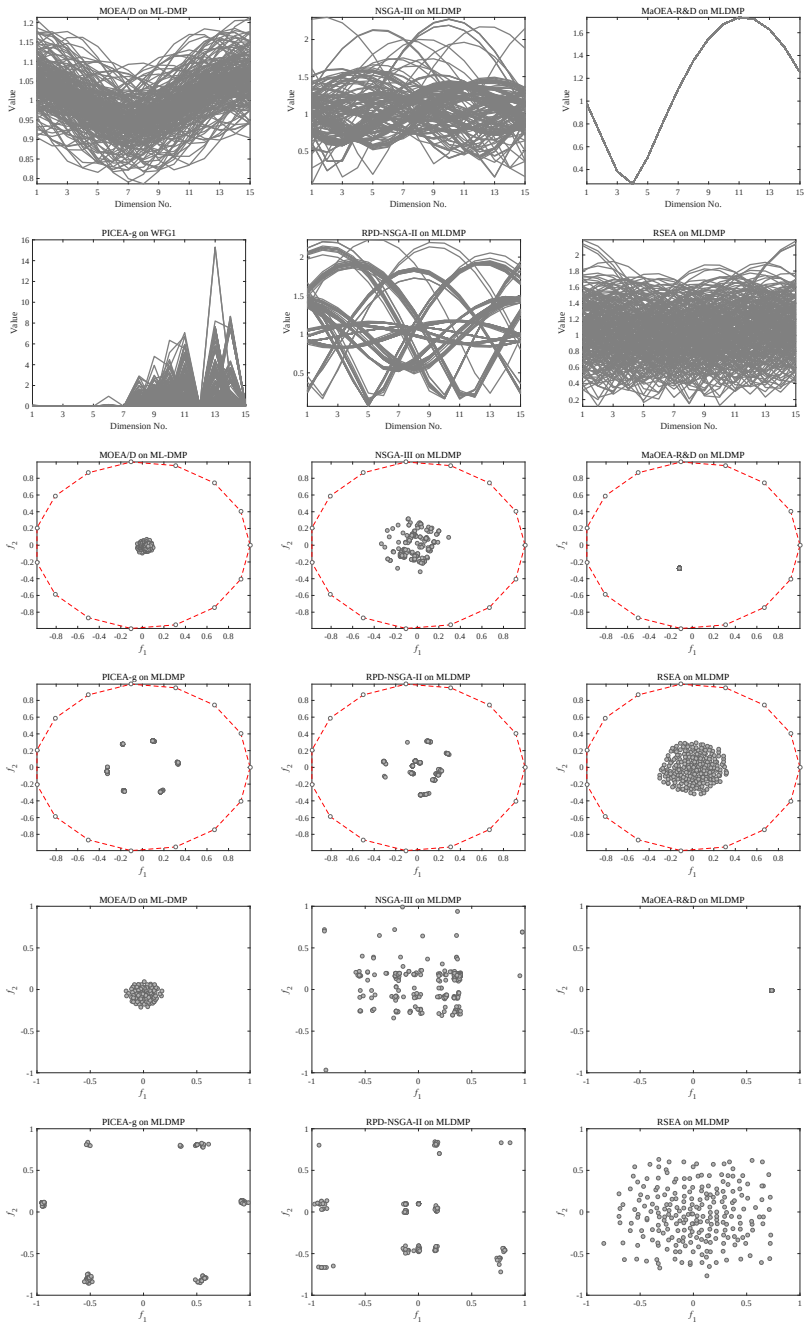

Figure 9: The non-dominated front obtained by each algorithm on ML-DMP with 15 objectives in the run associated with the median HV value are displayed by parallel coordinates and RadViz, respectively. The obtained decision vectors of each algorithm are also displayed to show the diversity maintenance of different algorithms.

4.7. Impact of the Permutation of Projection Weight Vectors

In RSEA, two projection weight vectors are adopted to project the high-dimensional objective vectors into the 2-dimensional radial space. We can see from Eq. (3) that the Euclidean distance of two solutions in radial space is related to these projection weight vectors. Hence, it is essential to test the effect of the permutation of elements in the projection weight vectors to the performance of RSEA. In this section, the RSEA with fixed projection weight vectors (the original defined projection weight vectors), the version with varying projection weight vectors (namely RSEA*, where the permutation of projection varies along with the evolution of the population), and the version with the inverted but fixed projection weight vectors (namely RSEA^T, where the original defined projection weight vectors are inverted) are compared on seven test problems selected from test suites DTLZ and WFG. The IGD values of the non-dominated solutions obtained by RSEA, RSEA*, and RSEA^T on different test instances are given in Table 10. In this table, RSEA and RSEA^T outperform RSEA* on DTLZ1,7, and WFG1,3,4 with 3, 5, and 10 objectives, while RSEA* performs the best on 3-, 5-objective DTLZ2 problem and 3-objective DTLZ5 problem. Meanwhile, RSEA performs similarly with RSEA^T on all the test instances, which means the fixed projection weight vectors will not effect the performance of RSEA. In conclusion, the variation in the permutation of the elements in the projection weight vectors will weaken the performance of RSEA, which may due to the fact that the diversity assess criterion provided by the radial projection may be messed with the varying projection weight vectors, while RSEA with fixed projection weight vectors does not suffer from this mess.

In Table 10, RSEA has achieved the most best results on 21 test instances. Generally speaking, RSEA and RSEA^T are overall outperforming RSEA* on most test problems, and the fixed projection weight vectors will not effect the performance of the proposed algorithm on solving MaOPs.

Table 10: The IGD Values Obtained by RSEA*, RSEA^T and RSEA on 21 Test Instances. The Best Result in Each Row is Highlighted.

Problem	Obj.	RSEA*	RSEA^T	RSEA
DTLZ1	3	2.01e-2(1.78e-4)−	2.00e-2(7.85e-5)≈	2.00e-2(8.45e-5)
	5	8.86e-2(4.70e-2)−	8.50e-2(3.86e-2)≈	7.55e-2(2.47e-3)
	10	3.41e-1(1.77e-1)≈	4.08e-1(2.23e-1)≈	3.61e-1(1.66e-1)
DTLZ2	3	5.33e-2(3.47e-4)−	5.28e-2(3.28e-4)≈	5.27e-2(2.85e-4)
	5	2.38e-1(5.54e-3)−	2.32e-1(5.16e-3)≈	2.33e-1(5.54e-3)
	10	4.55e-1(5.78e-3)+	4.67e-1(8.52e-3)≈	4.64e-1(7.24e-3)
DTLZ5	3	6.37e-3(6.37e-4)−	5.42e-3(5.18e-4)≈	5.31e-3(3.73e-4)
	5	8.91e-2(3.29e-2)+	1.47e-1(3.13e-2)≈	1.46e-1(3.11e-2)
	10	2.61e-1(9.73e-2)+	4.06e-1(8.83e-2)≈	4.06e-1(9.34e-2)
DTLZ7	3	7.77e-2(6.40e-2)+	7.54e-2(6.45e-2)≈	1.05e-1(1.07e-1)
	5	3.63e-1(4.69e-2)−	3.29e-1(5.11e-2)≈	3.30e-1(3.80e-2)
	10	1.90e+0(2.87e-1)−	1.70e+0(2.38e-1)≈	1.74e+0(1.82e-1)
WFG1	3	1.80e-1(2.58e-2)−	1.60e-1(1.18e-2)−	1.54e-1(1.49e-2)
	5	9.69e-1(1.47e-1)−	7.33e-1(7.02e-2)≈	7.30e-1(5.81e-2)
	10	1.57e+0(1.12e-1)−	1.44e+0(6.86e-2)≈	1.44e+0(8.28e-2)
WFG3	3	1.09e-1(1.17e-2)−	9.69e-2(7.04e-3)≈	9.80e-2(9.75e-3)
	5	4.48e-1(4.69e-2)−	3.21e-1(2.89e-2)≈	3.21e-1(3.08e-2)
	10	4.62e-1(1.65e-1)≈	4.21e-1(4.67e-2)≈	4.09e-1(4.20e-2)
WFG4	3	2.16e-1(2.24e-3)≈	2.15e-1(2.58e-3)≈	2.15e-1(2.24e-3)
	5	1.29e+0(4.36e-2)≈	1.29e+0(3.11e-2)≈	1.28e+0(1.86e-2)
	10	4.34e+0(8.92e-2)≈	4.34e+0(7.35e-2)≈	4.36e+0(8.94e-2)

5. Conclusions and discussion

In this paper, we have proposed a radial space division based evolutionary algorithm, called RSEA, for many-objective optimization. In the proposed RSEA, the radial projection is applied to project high dimensional objective vectors into the 2-dimensional radial space for diversity maintenance, which is inspired from the ability of RadViz on reflecting the distribution of high-dimensional points in a 2-dimensional radial space. To the best of our knowledge, this is the first time that the radial projection is used to project high-dimensional objective vectors into a 2-dimensional radial space for diversity maintenance in many-objective optimization.

In RSEA, an adaptive grid division strategy for selecting a set of uniformly distributed solutions in the radial space is developed, which is capable of maintaining the diversity of the population via the diversity maintenance in the 2-dimensional radial space. Despite of this adaptive grid division strategy in environmental selection, a binary tournament selection strategy using the crowding degree (in radial space) and convergence degree (in objective space) is adopted in mating selection to select the solutions with better convergence and good diversity, which is likely to reproduce promising offspring solutions for the next generation.

Results of comparison experiment on five state-of-the-art MaOEAs, namely, MOEA/D, NSGA-III, MaOEA-R&D, PICEA-g, and RPD-NSGA-II demonstrate that the proposed RSEA significantly outperforms MaOEA-R&D, PICEA-g, and RPD-NSGA-II on DTLZ test suite, and it outperforms all the compared MaOEAs on WFG test suite. Moreover, the performance of RSEA on MaF2, 4, 5 and ML-DMPs overall outperforms the other compared algorithms. Therefore, the overall performance of RSEA is highly competitive compared to the state-of-the-art MaOEAs for many-objective optimization.

This work demonstrates that the idea of radial space division based diversity maintenance strategy for many-objective optimization is very promising. Future work on improving the convergence maintaining ability together with the diver-

sity maintenance ability based on the radial projection is highly desirable. In RSEA, the environmental selection strategy only select a set of well distributed projected solutions, however, the performance of RSEA could be further improved by introducing convergence maintenance strategy incorporating with the diversity maintenance strategy in the radial projection based environmental selection. In addition, the application of RSEA on real-world problems remains to be verified.

Acknowledgment

Paper written during a six months stay of C. He in the Department of Computing, University of Surrey, UK, in the end of 2016 and the beginning of 2017, supported by National Natural Science Foundation of China (61320106005, 61502004, 61502001, and 61672033) and the Innovation Scientists and Technicians Troop Construction Projects of Henan Province (154200510012). The authors are grateful for Handing Wang's comments on the paper.

References

[1] R. J. Lygoe, M. Cary, P. J. Fleming, A real-world application of a many-objective optimisation complexity reduction process, in: Evolutionary Multi-Criterion Optimization, Springer, 2013, pp. 641–655.

[2] G. Li, H. Hu, Risk design optimization using many-objective evolutionary algorithm with application to performance-based wind engineering of tall buildings, Structural Safety 48 (2014) 1–14.

[3] J. B. Kollat, P. M. Reed, R. Maxwell, Many-objective groundwater monitoring network design using bias-aware ensemble kalman filtering, evolutionary optimization, and visual analytics, Water Resources Research 47 (2) (2011) 155–170.

[4] S. Chand, M. Wagner, Evolutionary many-objective optimization: a quick-start guide, Surveys in Operations Research and Management Science 20 (2) (2015) 35–42.

[5] B. Li, J. Li, K. Tang, X. Yao, Many-objective evolutionary algorithms: a survey, ACM Computing Surveys (CSUR) 48 (1) (2015) 13.

[6] P. J. Fleming, R. C. Purshouse, R. J. Lygoe, Many-objective optimization: an engineering design perspective, in: Proceedings of the International Conference on Evolutionary multi-criterion optimization, Springer, 2005, pp. 14–32.

[7] C. A. C. Coello, Evolutionary multi-objective optimization: a historical view of the field, IEEE Computational Intelligence Magazine 1 (1) (2006) 28–36.

[8] M. Farina, P. Amato, On the optimal solution definition for many-criteria optimization problems, in: Proceedings of the NAFIPS-FLINT International Conference, 2002, pp. 233–238.

[9] Q. Zhang, H. Li, MOEA/D: A multiobjective evolutionary algorithm based on decomposition, IEEE Transactions on Evolutionary Computation 11 (6) (2007) 712–731.

[10] H. Ishibuchi, N. Tsukamoto, Y. Nojima, Evolutionary many-objective optimization: A short review, in: IEEE Congress on Evolutionary Computation, Citeseer, 2008, pp. 2419–2426.

[11] K. Deb, A. Pratap, S. Agarwal, T. Meyarivan, A fast and elitist multiobjective genetic algorithm: NSGA-II, IEEE Transactions on Evolutionary Computation 6 (2) (2002) 182–197.

[12] E. Zitzler, M. Laumanns, L. Thiele, SPEA2: Improving the strength Pareto evolutionary algorithm (2001).

[13] H. Zhang, A. Zhou, S. Song, Q. Zhang, X. Gao, J. Zhang, A self-organizing multiobjective evolutionary algorithm, IEEE Transactions on Evolutionary Computation 20 (5) (2016) 792–806.

[14] R. Denysiuk, L. Costa, I. E. Santo, J. C. Matos, MOEA/PC: Multiobjective evolutionary algorithm based on Polar coordinates, in: International Conference on Evolutionary Multi-Criterion Optimization, Springer, 2015, pp. 141–155.

[15] D. W. Corne, N. R. Jerram, J. D. Knowles, M. J. Oates, PESA-II: Region-based selection in evolutionary multi-objective optimization, in: Proceedings of the genetic and evolutionary computation conference (GECCO2001), Citeseer, 2001, pp. 283–290.

[16] R. C. Purshouse, P. J. Fleming, On the evolutionary optimization of many conflicting objectives, IEEE Transactions on Evolutionary Computation 11 (6) (2007) 770–784.

[17] R. Cheng, Y. Jin, M. Olhofer, B. Sendhoff, A reference vector guided evolutionary algorithm for many-objective optimization, IEEE Transactions on Evolutionary Computation 20 (2016) 773–791.

[18] G. Wang, H. Jiang, Fuzzy-dominance and its application in evolutionary many objective optimization, in: Proceedings of the 2007 International Conference on Computational Intelligence and Security Workshops, IEEE, 2007, pp. 195–198.

[19] M. Laumanns, L. Thiele, K. Deb, E. Zitzler, Combining convergence and diversity in evolutionary multiobjective optimization, Evolutionary Computation 10 (3) (2002) 263–282.

[20] M. Elarbi, S. Bechikh, A. Gupta, L. B. Said, Y.-S. Ong, A new decomposition-based NSGA-II for many-objective optimization, IEEE Transactions on Systems, Man, and Cybernetics: Systems (2017) in press.

[21] F. di Pierro, S.-T. Khu, D. A. Savić, An investigation on preference order ranking scheme for multiobjective evolutionary optimization, IEEE Transactions on Evolutionary Computation 11 (1) (2007) 17–45.

[22] X. Zhang, Y. Tian, Y. Jin, A knee point driven evolutionary algorithm for many-objective optimization, IEEE Transactions on Evolutionary Computation 19 (6) (2015) 761–776.

[23] S. Yang, M. Li, X. Liu, J. Zheng, A grid-based evolutionary algorithm for many-objective optimization, IEEE Transactions on Evolutionary Computation 17 (5) (2013) 721–736.

[24] K. Deb, H. Jain, An evolutionary many-objective optimization algorithm using reference-point-based nondominated sorting approach, part I: Solving problems with box constraints, IEEE Transactions on Evolutionary Computation 18 (4) (2014) 577–601.

[25] K. Li, K. Deb, Q. Zhang, S. Kwong, An evolutionary many-objective optimization algorithm based on dominance and decomposition, IEEE Transactions on Evolutionary Computation 19 (5) (2015) 694–716.

[26] Y. Yuan, H. Xu, B. Wang, B. Zhang, X. Yao, Balancing convergence and diversity in decomposition-based many-objective optimizers, IEEE Transactions on Evolutionary Computation 20 (2) (2016) 180–198.

[27] R. Wang, R. C. Purshouse, P. J. Fleming, Preference-inspired coevolutionary algorithms for many-objective optimization, IEEE Transactions on Evolutionary Computation 17 (4) (2013) 474–494.

[28] E. Zitzler, S. Künzli, Indicator-based selection in multiobjective search, in: Proceedings of the International Conference on Parallel Problem Solving from Nature, Springer, 2004, pp. 832–842.

[29] N. Beume, B. Naujoks, M. Emmerich, SMS-EMOA: multiobjective selection based on dominated hypervolume, European Journal of Operational Research 181 (3) (2007) 1653–1669.

[30] J. Bader, E. Zitzler, HypE: an algorithm for fast hypervolume-based many-objective optimization, Evolutionary computation 19 (1) (2011) 45–76.

[31] R. Hernández Gómez, C. A. Coello Coello, Improved metaheuristic based on the R2 indicator for many-objective optimization, in: Proceedings of the 2015 Annual Conference on Genetic and Evolutionary Computation, ACM, 2015, pp. 679–686.

[32] Y. Tian, X. Zhang, R. Cheng, Y. Jin, A multi-objective evolutionary algorithm based on an enhanced inverted generational distance metric, in: 2016 IEEE Congress on Evolutionary Computation (CEC), IEEE, 2016, pp. 5222–5229.

[33] H. Wang, L. Jiao, X. Yao, Two_arch2: An improved two-archive algorithm for many-objective optimization, IEEE Transactions on Evolutionary Computation 19 (4) (2015) 524–541.

[34] X. Zhang, Y. Tian, Y. Jin, R. Cheng, A decision variable clustering-based evolutionary algorithm for large-scale many-objective optimization, IEEE Transactions on Evolutionary Computation (2016) in press.

[35] Q. Lin, S. Liu, Q. Zhu, C. Tang, R. Song, J. Chen, C. A. C. Coello, K.-C. Wong, J. Zhang, Particle swarm optimization with a balanceable fitness estimation for many-objective optimization problems, IEEE Transactions on Evolutionary Computation.

[36] H. Wang, Y. Jin, X. Yao, Diversity assessment in many-objective optimization, IEEE Transactions on Cybernetics (2016) in press.

[37] L. Pan, C. He, Y. Tian, Y. Su, X. Zhang, A region division based diversity maintaining approach for many-objective optimization, Integrated Computer-Aided Engineering (2017) in press.

[38] S. Jiang, S. Yang, A strength Pareto evolutionary algorithm based on reference direction for multi-objective and many-objective optimization, IEEE Transactions on Evolutionary Computation (2016) in press.

[39] M. Asafuddoula, T. Ray, R. Sarker, A decomposition based evolutionary algorithm for many objective optimization, IEEE Transactions on Evolutionary Computation 19 (3) (2015) 445–460.

[40] F. Gu, Y. Cheung, Self-organizing map-based weight design for decomposition-based many-objective evolutionary algorithm, IEEE Transactions on Evolutionary Computation (2017) in press.

[41] T. Tušar, B. Filipič, Visualization of Pareto front approximations in evolutionary multiobjective optimization: A critical review and the prosection method, IEEE Transactions on Evolutionary Computation 19 (2) (2015) 225–245.

[42] Z. He, G. G. Yen, Visualization and performance metric in many-objective optimization, IEEE Transactions on Evolutionary Computation 20 (3) (2016) 386–402.

[43] M. Ashby, Multi-objective optimization in material design and selection, Acta Materialia 48 (1) (2000) 359–369.

[44] T. Kohonen, The self-organizing map, Neurocomputing 21 (1) (1998) 1–6.

[45] A. R. Martin, M. O. Ward, High dimensional brushing for interactive exploration of multivariate data, in: Proceedings of the 6th Conference on Visualization'95, IEEE Computer Society, 1995, p. 271.

[46] J. B. Tenenbaum, V. De Silva, J. C. Langford, A global geometric framework for nonlinear dimensionality reduction, Science 290 (5500) (2000) 2319–2323.

[47] J. W. Sammon, A nonlinear mapping for data structure analysis, IEEE Transactions on Computers 18 (5) (1969) 401–409.

[48] P. Hoffman, G. Grinstein, K. Marx, I. Grosse, E. Stanley, DNA visual and analytic data mining, in: Proceedings of Visualization'97, IEEE, 1997, pp. 437–441.

[49] L. V. D. Maaten, G. Hinton, Visualizing data using t-SNE, Journal of Machine Learning Research 9 (Nov) (2008) 2579–2605.

[50] A. Pryke, S. Mostaghim, A. Nazemi, Heatmap visualization of population based multi objective algorithms, in: Evolutionary Multi-Criterion Optimization, Springer, 2007, pp. 361–375.

[51] M. Köppen, K. Yoshida, Substitute distance assignments in nsga-ii for handling many-objective optimization problems, in: International Conference on Evolutionary Multi-Criterion Optimization, Springer, 2007, pp. 727–741.

[52] D. J. Walker, R. Everson, J. E. Fieldsend, Visualizing mutually nondominating solution sets in many-objective optimization, IEEE Transactions on Evolutionary Computation 17 (2) (2013) 165–184.

[53] A. Ibrahim, S. Rahnamayan, M. V. Martin, K. Deb, 3D-RadVis: Visualization of Pareto front in many-objective optimization, in: Proceedings of the 2016 IEEE Congress on Evolutionary Computation (CEC), IEEE, 2016, pp. 736–745.

[54] X. Zhang, Y. Tian, R. Cheng, Y. Jin, An efficient approach to nondominated sorting for evolutionary multi-objective optimization, IEEE Transactions on Evolutionary Computation 19 (2) (2015) 201–213.

[55] Z. He, G. G. Yen, Many-objective evolutionary algorithm: objective space reduction + diversity improvement, IEEE Transactions on Evolutionary Computation 20 (1) (2016) 145–160.

[56] Y. Tian, R. Cheng, X. Zhang, Y. Jin, Platemo: A MATLAB platform for evolutionary multi-objective optimization, arXiv preprint arXiv:1701.00879.

[57] K. Deb, L. Thiele, M. Laumanns, E. Zitzler, Scalable test problems for evolutionary multiobjective optimization, Advanced Information and Knowledge Processing, Springer London, 2005.

[58] L. B. S. Huband, P. Hingston, L. While, A review of multiobjective test problems and a scalable test problem toolkit, IEEE Transactions on Evolutionary Computation 10 (5) (2006) 477–506.

[59] R. Cheng, M. Li, Y. Tian, X. Zhang, S. Yang, Y. Jin, X. Yao, Benchmark functions for the cec'2017 competition on many-objective optimization, Tech. rep., University of Birmingham, UK (2017).

[60] M. Li, C. Grosan, S. Yang, X. Liu, X. Yao, Multi-line distance minimization: A visualized many-objective test problem suite, IEEE Transactions on Evolutionary Computation (2017) in press.

[61] A. Zhou, Y. Jin, Q. Zhang, B. Sendhoff, E. Tsang, Combining model-based and genetics-based offspring generation for multi-objective optimization using a convergence criterion, in: Proceedings of the 2006 IEEE Congress on Evolutionary Computation, 2006, pp. 892–899.

[62] C. He, L. Pan, H. Xu, Y. Tian, X. Zhang, An improved reference point sampling method on pareto optimal front, in: Proceedings of the 2016 IEEE Congress on Evolutionary Computation (CEC), IEEE, 2016, pp. 5230–5237.

[63] L. While, P. Hingston, L. Barone, S. Huband, A faster algorithm for calculating hypervolume, IEEE Transactions on Evolutionary Computation 10 (1) (2006) 29–38.

[64] K. Deb, Multi-Objective Optimization Using Evolutionary Algorithms, New York: Wiley, 2001.

[65] K. Deb, M. Goyal, A combined genetic adaptive search (geneas) for engineering design, Computer Science and Informatics 26 (1996) 30–45.

[66] K. Deb, Multi-objective optimization using evolutionary algorithms, Vol. 16, John Wiley & Sons, 2001.

[67] I. Das, J. E. Dennis, Normal-boundary intersection: A new method for generating the pareto surface in nonlinear multicriteria optimization problems, SIAM Journal on Optimization 8 (3) (1998) 631–657.